Ind. J. Pharm. Edu. Res., 2026; 60(3):1096-1112.
https://www.ijper.org

Original Article

Anti-cancer and Apoptotic Effects of Juglone in Ovarian Carcinoma: An Integrated Computational and Experimental Study

Mei Wu[1,#], QinJian Xia[2,#], Lihui Liu[3], Le Kang[4,*]

[1]Department of Gynecology, Jingzhou Hospital of Traditional Chinese Medicine, Jingzhou, Hubei, CHINA.
[2]Department of Gynecology, Nantong Haimen People's Hospital, Nantong, Jiangsu, CHINA.
[3]Department of Outpatient, General Hospital of the Western Theater Command of Chinese People's Liberation Army, Sichuan, Chengdu, CHINA.
[4]Department of Gynecology and Obstetrics, Huai'an Clinical Medical College of Jiangsu University (Huai'an Hospital of Huai'an City), Huai'an, Jiangsu, CHINA.
[#]Mei Wu and QinJian Xia are co-first authors, they contributed equally to this work.

ABSTRACT

Background: Juglone, a naturally occurring naphthoquinone, has been recognized for its potential anticancer properties. Recent advances in network pharmacology allow for the systematic elucidation of complex molecular interactions in disease, particularly in oncology. **Objectives:** This study aimed to integrate network pharmacology, *in silico* molecular docking and experimental validation to demonstrate the anticancer potential of juglone in OVCAR-3 human ovarian carcinoma cells. **Materials and Methods:** SwissADME and Pro-Tox 3.0 assessed the physicochemical and toxicological properties of juglone. Protein targets were predicted using the SwissTargetPrediction and Super-PRED servers, while ovarian cancer targets were retrieved from the GeneCards database. Common targets were identified via the Venny online tool and Protein-Protein Interaction (PPI) networks were constructed to reveal key targets and connectivity. Functional annotations and enrichment analyses were conducted using bioinformatics software and GEPIA-2 performed expression analysis of hub genes in tumor versus normal tissues. The identified hub genes were subjected to molecular docking to evaluate non-covalent interactions with juglone. *In vitro* assays included MTT (3-(4,5-Dimethylthiazol-2-yl)-2,5-Diphenyltetrazolium-Bromide), Annexin V/PI and flowcytometry for cytotoxicity, apoptosis and cell cycle against OVACAR-3 cells, respectively. **Results:** SwissADME revealed juglone's favorable ADME (bioavailability=0.55, high GI absorption, BBB permeability) and Pro-Tox 3.0 confirmed its safety. Target prediction (SwissTargetPrediction, Super-PRED) identified 107 juglone targets versus 1242 ovarian cancer targets (GeneCards), yielding 26 common targets via Venny. A PPI network (26 nodes, 153 edges) identified hub genes as HDAC2, CDK2, STAT3 and CDK1. GEPIA showed CDK1 overexpression with poor prognosis. Docking on HDAC2, CDK2, CDK1 produced binding energies of -7.1, -7.6 and -5.6 kcal/mol, respectively. MTT assay confirmed that juglone induced concentration-dependent cytotoxicity in OVCAR-3 ovarian cancer cells. Apoptosis and cell cycle assays demonstrated early/late apoptosis and G2/M phase arrest. **Conclusion:** The bioinformatics and experimental findings provide significant evidence of cytotoxic, apoptotic and cell cycle arrest properties in human ovarian carcinoma for juglone.

Keywords: Cell Cycle Arrest, Juglone, Molecular Docking, Network Pharmacology, Ovarian Cancer.

Correspondence:
Dr. Le Kang
Department of Gynecology and Obstetrics, Huai'an Clinical Medical College of Jiangsu University (Huai'an Hospital of Huai'an City), Huai'an,-223200, Jiangsu, CHINA.
Email: kangle1888@outlook.com
ORCID: 0009-0002-6128-1582

Received: 07-12-2025;
Revised: 27-02-2026;
Accepted: 15-04-2026.

INTRODUCTION

Globally, ovarian carcinoma is still the primary cause of cancer-related death in women, which necessitates the search for new treatment options.[1] Juglone belongs to the naphthoquinone class of natural products and is chemically 5-hydroxy-1,4-naphthoquinone isolated from the different parts of the walnut tree like roots, bark, leaves and has received huge interest due to its multidimensional pharmacological properties, especially its anticancer potential. Juglone is an antioxidant compound and as such can help prevent oxidative stress by generating reactive oxygen species. It can also act as a redox cycling agent due to its quinone structure. The pro-oxidant properties of juglone can also have cancer cell killing effect and as such can have positive impact on health. Juglone has been reported to exhibit anticancer effects in a range of human malignancies like cervical cancer, breast cancer, brain cancer and lung cancer. Juglone has been found to

DOI: 10.5530/ijper.20261749

exhibit anticancer action by inhibiting cancer cell proliferation, induction of tumor cell apoptosis, autophagy induction, inhibition of angiogenesis as well as suppression of cancer cell migration and invasion.[2-5] Juglone has also been reported to induce apoptosis and autophagy through the activation of ROS-mediated p53 pathway under *in vitro* and *in vivo* conditions in human liver carcinoma. Juglone has been reported to induce programmed cell death by increasing ROS (reactive oxygen species) generation, which leads to oxidative stress which in turn activates the PI3K/Akt signaling pathway leading to cancer cell death.[6-8] Juglone has also been reported to induce G2/M phase cell cycle arrest in HepG2 cells (liver carcinoma) and OVCAR-3 cells (ovarian cancer).[9,10]

Network pharmacology has emerged as a pivotal tool in anticancer research, especially for investigating natural products. It elucidates the intricate interactions between drugs and their biological targets, highlighting crucial protein targets and pathways. By constructing interaction networks, network pharmacology reveals how drugs modulate various biological processes such as the cell cycle, apoptosis, metastasis and necrosis. It also identifies target genes and links them to pathways through Gene Ontology (GO) and Kyoto Encyclopedia of Genes and Genomes (KEGG) enrichment analysis. By integrating biological data and computational methods, network pharmacology effectively identifies multiple targets of natural products and complex plant extracts, addressing a previously challenging task.[11-13] This approach has revolutionized TCM by validating its multiherb, multicompound prescriptions, helping to identify active ingredients and their precise molecular targets. Consequently, it enhances both safety and efficacy by predicting drugdrug interactions and toxicities. Moreover, natural products are reevaluated as valuable leads and novel mechanisms emerge from their networkbased analysis. Network pharmacology has become pivotal in elucidating the multi-target mechanisms underlying traditional medicinal formulations in cancer therapy. Shang *et al.*, (2023) combined computational predictions with experimental validation to detail how Sijunzi Decoction modulates colorectal cancer pathways.[14] Yuan *et al.*, (2021) applied network pharmacology and molecular docking to uncover the mechanism by which Scopoletin interferes with non-small cell lung cancer progression.[15] Similarly, He *et al.*, (2023) used these approaches to reveal multi-target actions of curcumin against colon cancer.[16]

Ovarian carcinoma remains a leading cause of gynecological cancer mortality, necessitating novel therapeutic strategies. Juglone, a natural quinone, exhibits potential anticancer properties, but its precise molecular mechanisms in ovarian cancer remain unexplored. This study integrates computational chemistry, bioinformatics and experimental assays to elucidate apoptotic and anticancer effects of juglone. By combining *in silico* docking, molecular dynamics and experimental validation, we provide comprehensive theoretical and experimental evidence. The novelty lies in the multi-disciplinary approach, offering mechanistic insights into interaction of juglone with key oncogenic targets, which could pave the way for novel therapeutic interventions in ovarian carcinoma treatment.

MATERIALS AND METHODS

Physicochemical evaluation and biological targets of juglone and ovarian cancer

Using the juglone SMILE formula, which was retrieved from https://pubchem.ncbi.nlm.nih.gov/, the druglikeness, bioavailability, Blood Brain Barrier (BBB) and Gastrointestinal absorption (GI) parameters were determined by inputting it into the http://www.swissadme.ch/index.php (SwissADME) website.[17] The biological targets of juglone were also obtained from the Super-PRED (https://prediction.charite.de/index.php) and the Swiss Target Prediction databases (http://www.swisstargetprediction.ch).[18,19] Utilising UniProt (http://www.uniprot.org), the anticipated target names and IDs were obtained, limiting the species to "*Homo sapiens*". Using "ovarian cancer" as the keyword, we obtained the target genes associated with ovarian cancer from the GeneCards database (https://www.genecards.org).[20,21] The retrieved gene names were renamed to their official (preferred) names using Uniprot data. The resulting juglone and ovarian cancer targets were overlapped and intersected using the Venn diagram from the venny (2.1) web tool. Juglone targets and the ovarian cancer targets that were common were subjected to further network analysis.

Network construction

The overlapping/intersecting genes were added to the STRING database (https://string-db.org), a search engine based on bioinformatics that helps find interacting proteins and genes.[22] As a result, Protein-Protein Interaction (PPI) networks that satisfied the prerequisite of having a confidence score higher than 0.4 could be created. The most significant genes were identified by importing the protein interaction network into Cytoscape Software, Version 3.10.2. With the Cyto Hubba plugin in Cytoscape, we generated and analysed a hub-genes network diagram. Further, the active compound (juglone)-protein target-signalling pathway network was constructed using Cytoscape software which identified the main biological targets of juglone and their association with various signalling pathways involved in ovarian cancer.

Gene Ontology (GO) and Kyoto Encyclopedia of Genes and Genomes (KEGG) pathway enrichment analysis

By using the GO database (www.geneontology.org), the possible biological mechanisms of therapeutic action of juglone which consist of Molecular Function (MF), Cellular Component (CC) and Biological Process (BP) terms were identified considered

significant at $p<0.05$. The therapeutic targets and their association with the key signalling pathways were explored by using KEGG database (www.kegg.jp). The GO and KEGG enrichment analysis was performed by using the bioinformatics software (www.bioinformatics.com.cn).

In silico molecular docking

In silico molecular docking has become a significant tool in computational drug discovery and design. We used molecular docking to identify various non-covalent interactions and their strength formed between juglone and the amino acid residues of the active sites of the four hub targets including HDAC2, CDK2, CDK1 and STAT3. Docking analysis was performed using CB-Dock (https://cadd.labshare.cn/cb-dock2/index.php) online tool. CB-Dock is a blind docking technique which automatically identifies the sites for binding to a particular protein site and then carry out docking using AutoDock. It has been demonstrated that CB-Dock outperforms other state-of-the-art blind docking approaches in precisely predicting binding structures and locations.[23,24] The Protein Data Bank (http://www.rcsb.org) provided the crystal structures of the hub protein targets for download. Using the PubChem Compound database (https://www.ncbi.nlm.nih.gov), the 3D structure of juglone (ligand) was obtained. Next, the files including the protein (receptor) and juglone (ligand) were uploaded to the CB-Dock website for molecular docking analysis.

Survival analysis and differential expression of the hub targets

In order to understand the prognostic value of juglone in individuals with ovarian cancer, we carried out survival analysis. In order to find possible therapeutic targets related to the prognosis of ovarian cancer patients, the four hub targets (HDAC2, CDK2, CDK1 and STAT3) were uploaded into the GEPIA database (http://gepia.cancer-pku.cn).[25]

Experimental validation

MTT assay for assessing cell viability

The human ovarian cancer cells OVCAR-3 (Cat. no. HTB-161; ATCC) were grown overnight in RPMI medium (Sigma-Aldrich St. Louis, MO, USA). Penicillin-streptomycin (Gibco, Greenville, USA) and 10% Foetal Bovine Serum (FBS; Gibco, Greenville, USA) were subsequently added to the medium. The cells were kept at 37°C with 5% CO_2 in an incubator. Using the MTT assay, the viability of the OVCAR-3 cells was assessed 24 and 48 hr after they were exposed to different juglone concentrations (0, 15, 30, 60 and 120 µM). Following treatment with juglone, 10^4 cells per well in 96-well plates were cultivated for 8 hr using MTT 10 mg/mL; (Sigma-Aldrich St. Louis, MO, USA). A microplate reader was used to measure the absorbance at 540 nm following the solubilization of the Formazan crystals in DMSO (Sigma-Aldrich St. Louis, MO, USA). Viability was expressed as a percentage with 100% serving as the reference point for control cells treated with 0.1% DMSO.

Apoptosis assay using annexin V and flow cytometry

Using flow cytometry and annexin V-FITC/PI apoptosis detection kit (KeyGen Biotech Co. Ltd. Najing, China), human ovarian cancer cells were analysed to quantify apoptotic cells following increasing dose of juglone treatment. Cell cultures were stained using annexin V-FITC and PI (10 µL each) in a dark chamber at room temperature for approximately 15 min followed by treatment with different doses (0, 15, 60 and 120 µM) of juglone. In order to measure the extent of apoptosis in these cancer cells, each sample was finally examined using BD-FACSCalibur™ flow cytometry system (BD-Biosciences, San Jose, USA).

Cell cycle analysis

After being treated for 48 hr with different concentrations of juglone (0, 15, 60 and 120 µM), OVCAR-3 human ovarian cancer cells were collected and fixed with 70% ethanol for 12 hr at -20°C. Following a 20-min staining procedure with Propidium Iodide (PI) solution, the cells were analyzed using BD-FACSCalibur™ flow cytometry system (BD-Biosciences, San Jose, USA).

Table 1: Prediction of various physicochemical properties essential for a potential drug candidate using SwissADME, Toxicity was predicted by Pro-Tox 3.0. Juglone was predicted with high water solubility, good bioavailability, high gastrointestinal absorption with Blood Brain Barrier (BBB) permeability. No major toxicity was predicted.

Sl. No.	Descriptor	Value
1	Molecular Weight	174.155
2	LogP	1.3274
3	Rotatable Bonds	0
4	Hydrogen bond acceptors	3
5	Hydrogen bond donors	1
6	Surface Area	74.313
7	Water solubility	Soluble
8	Intestinal absorption (human)	High
9	Blood brain barrier (BBB) permeability	Yes
10	Bioavailability Score	0.55
11	Druglikeness	Yes, 0 violations from Lipinski rule of 5
12	Log Kp (skin permeation)	-6.00 cm/s
13	Hepatotoxicity	No
14	Neurotoxicity	No
15	Cytotoxic	Yes
16	Cardiotoxicity	No

Statistical Analysis

Using the one-way ANOVA test, followed by Tukey's *post hoc* test analysis, all the data were processed and analysed. The data were handled by GraphPad Prism 5 and a *p* value of ˂0.05 and ˂0.01 were considered as statistically significant. All the results were presented as Mean±Standard Error of Mean (SEM) of triplicate samples.

RESULTS

ADME properties, toxicity profile and Target prediction of juglone

The SwissADME online server was used to Determine the Physicochemical Properties (ADME) of juglone, including its bioavailability, GI absorption, BBB, druglikeness and partition coefficient. The bioavailability of the drug candidate was determined to be 0.55, with a high Gastrointestinal Absorption (GI) absorption. Juglone also exhibited blood brain barrier permeability which is not the case for most drugs as BBB permeability is very rare. The Pro-Tox 3.0 web server indicated that there was no significant toxicity linked to juglone, suggesting its safe nature. The toxicity and ADME characteristics of the juglone molecule are shown in Figure 1 and Table 1, respectively. Target prediction using Super-PRED and Swiss Target Prediction databases exhibited that 107 targets were identified for juglone (Supplementary Table S1).

Identification of ovarian cancer targets

Information on "ovarian cancer" which was the key word search term used to find the disease targets associated with ovarian cancer, was sourced from the GeneCards database. Apart from impeccably merging genomic, proteomic, genetic,

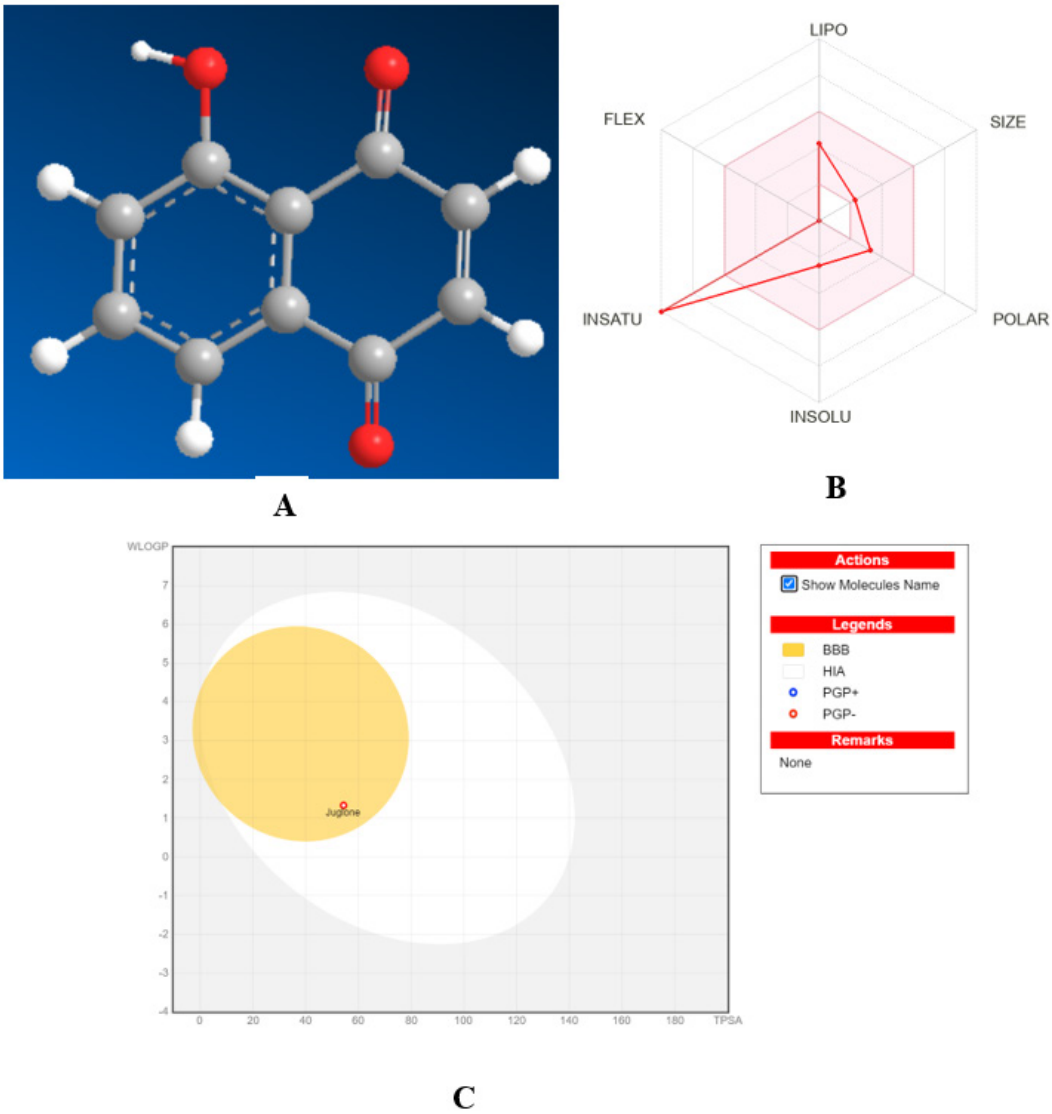

Figure 1: Prediction of physicochemical properties of juglone using SwissADME server, A shows the 3-D structure of juglone, B shows the radar of physicochemical properties of juglone, C shows the BIOLED-Egg model.

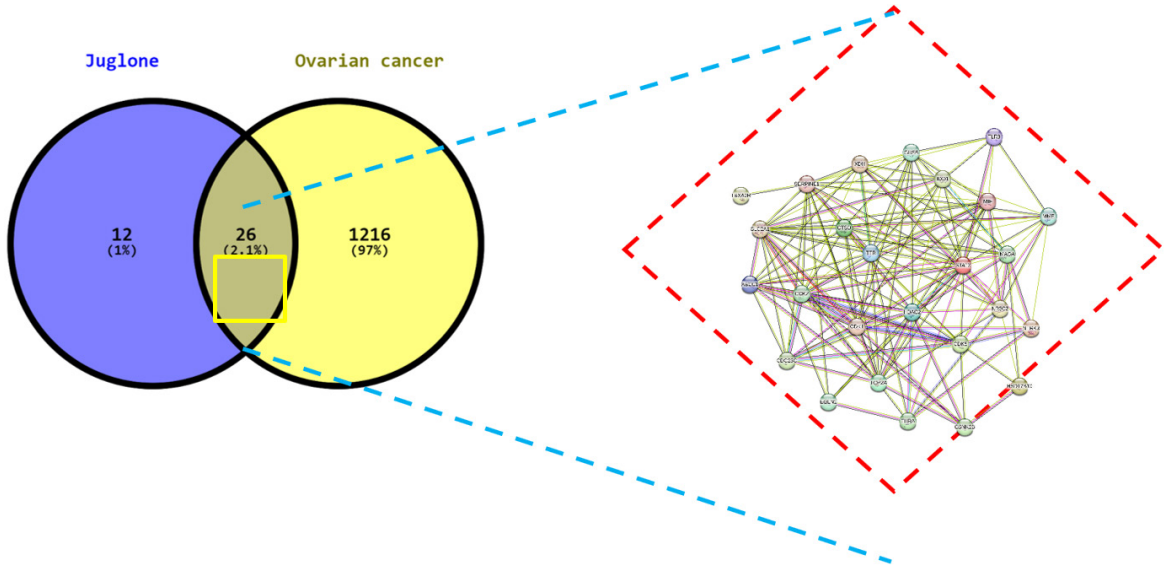

Figure 2: Illustration of the Protein-Protein Interaction (PPI) network of the common targets between juglone and ovarian cancer using a venn diagram constructed by using venny 2.0 online tool.

transcriptomic, functional and clinical data, GeneCards provides all annotated and predicted human genes with comprehensive and user-friendly accessibility.[26] The total number of identified targets linked to ovarian cancer were found to be 1242 after applying a 55 gift score filter to the initially retrieved 10392 total number of targets. Supplementary Table S2 depicts these 1242 number of targets for ovarian cancer.

Recognizing common targets between juglone and ovarian cancer

After feeding the individual targets of juglone and ovarian cancer into the venny online web tool, 26 common targets between juglone and ovarian cancer were identified which accounts for 2.1% of the total targets. These common targets along with the constructed Protein-Protein Interaction (PPI) network is depicted in Figure 2. The common targets in tabular form are provided in Supplementary Table S3. The main aim of identifying common targets between juglone and ovarian cancer stems from the fact that these common targets have the highest probability of being involved in the onset and progression of ovarian cancer and juglone molecule can exert therapeutic effect in ovarian cancer by modulating these targets. Additionally, we built a Protein-Protein Interaction (PPI) network using the STRING database, which shows which protein targets are connected to which other proteins and the degree of their association.

Construction of Protein-Protein Interaction (PPI) network and identification of hub genes

The PPI network was created and analysed by importing the 26 common genes from the STRING database. This PPI is explained in depth in Figure 3, which displays 153 edges, 26 nodes and an average node degree of 11.8. In a PPI network, target proteins are represented as nodes, while the edges show the relationships and connections between the proteins. A target protein with a higher degree value is thought to be more significant inside that PPI network. Hub genes exhibit a remarkably elevated degree values in a PPI network, signifying their importance within the network. Consequently, hub genes are pivotal in numerous biological processes and signalling pathways. This is why hub genes are important and exhibit close association with the disease. We found the following five hub genes using the Cyto Hubba plug in using Cytoscape software by following degree method: HDAC2 (node degree 6), CDK2 (node degree 6), CDK1 (node degree 5), STAT3 (node degree 5), MAOA (node degree 4). The pathways in cancer, the cell cycle, viral carcinogenesis and MicroRNAs in cancer were the four most important pathways found by Cyto Hubba and these pathways were directly affected by the above-mentioned hub genes. Figure 4 depicts the hub genes, how they interact with one another and the signalling pathways affected by these hub genes.

Construction of Juglone-target protein-signalling pathways network using Cytoscape

Using the Cytoscape 3.10.2 software program, a comprehensive network showing the relationship between juglone, its biological targets and the signalling pathways it affects was built. This visual network is depicted in Figure 5; The central red octagon shows juglone molecule, the light brown color squares represent the biological targets of juglone while as the green hexagons represent the signalling pathways involved in the therapeutic action of juglone in ovarian cancer. The network consists of 50 nodes with 74 edges with 2.96 average number of neighbors.

Gene Ontology (GO) and KEGG enrichment analysis

Understanding the genes involved and their roles in explaining the therapeutic impact of juglone in ovarian cancer is made

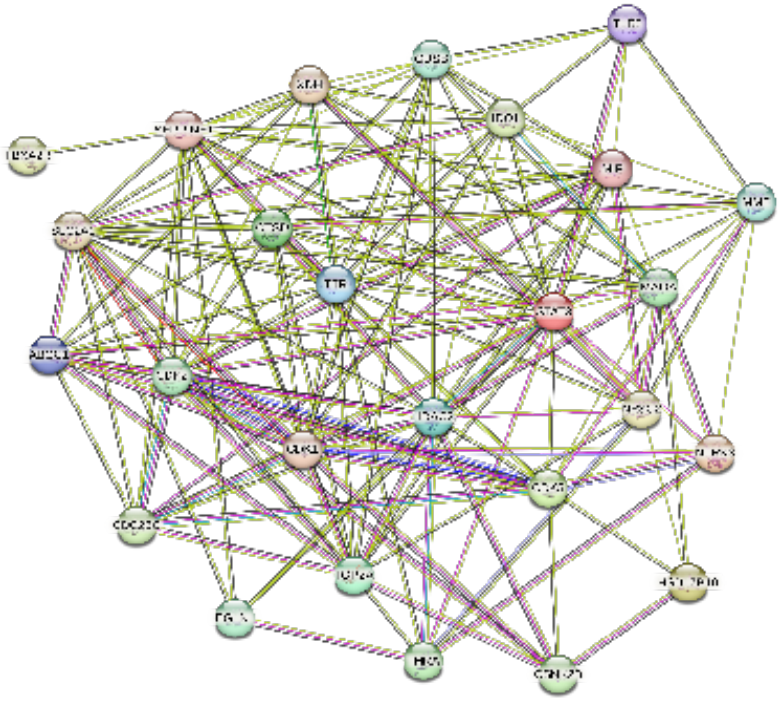

Figure 3: Protein-Protein Interaction (PPI) network of the common targets between juglone and ovarian cancer obtained using venny online portal in the form of a venn diagram.

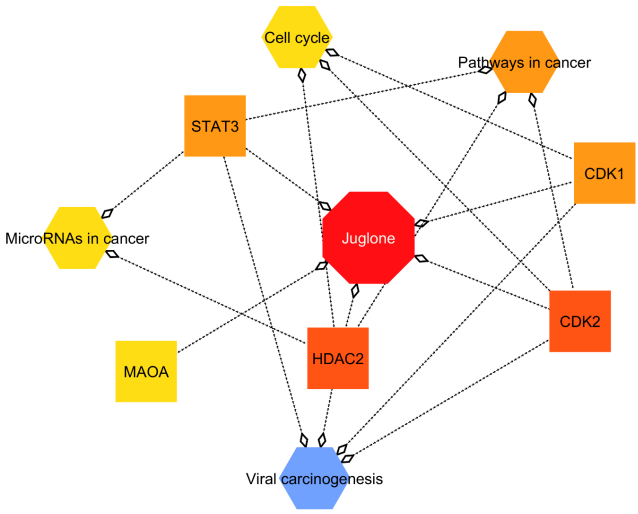

Figure 4: Construction of a network of hub genes using CytoHubba in Cytoscape software, depicting five most significant genes and signalling pathways involved in the therapeutic effect of juglone in ovarian cancer.

easier with the use of the Gene Ontology (GO) enrichment analysis. Twenty-six (26) predicted biological targets of juglone in the treatment of ovarian cancer were used in the current study. The three groups in the GO enrichment analysis are Biological Process (BP), Molecular Function (MF) and Cellular Component (CC). In our case, we identified 10 BPs, MFs and CCs and the most enriched BPs were signal transduction by p53 class mediator, regulation of signal transduction by p53 class mediator, neutrophil degranulation, neutrophil activation involved in immune response, negative regulation of cell migration, negative regulation of cell motility, regulation of cell cycle arrest. The most enriched MFs terms were nuclear receptor activity, ligand activated transcription factor activity, cyclin-dependent protein serine /threonine kinase activity, cyclin-dependent protein kinase activity, drug binding, chromatin DNA binding, DNA-binding transcription factor binding, RNA polymerase ll-specific DNA-binding transcription factor binding, p53 binding. The most enriched CC terms were secretory granule lumen, cytoplasmic vesicle lumen, vesicle lumen, ficolin-1-rich granule lumen, ficolin-1-rich granule, post-synaptic specialization. The GO analysis of all the BP, MF and CC are shown in Figure 6. The KEGG enrichment analysis

displaying the top 10 signalling pathways is shown in Figure 7. The main signalling pathways include cell cycle, HIF-1 signalling pathway, MicroRNAs in cancer, p53 signalling pathway, viral carcinogenesis, phenylalanine metabolism. The gene mapping diagrams Figure 8-a and Figure 8-b show the two most significant signalling pathways involved in the onset and progression of ovarian cancer along with showing the involved hub genes that were identified by Cytohubba. These pathways include cell cycle and pathways in cancer. This means that juglone molecule mostly targets cell cycle and several pathways in cancer in therapeutic effect against ovarian cancer.

Expression analysis and survival analysis of the key targets

Using data from the GEPIA database, an investigation was performed to analyse the expression and prognostic behaviour of three hub genes involved in ovarian cancer. Out of these only CDK1 gene was overexpressed in ovarian cancer tissues as compared to the normal tissues. Red boxes indicate Tumor (T) tissues while as green boxes indicate Normal (N) tissues, $*p<0.05$. The other survival analysis plots indicate how overexpression is associated with disease prognosis. For HDAC2 and CDK2, there was only a minute difference between the expression levels of the tumor and normal tissues. Further, the overexpression of CDK1 also had a significant impact on the Overall Survival (OS) and Disease-Free Survival (DFS) of the ovarian cancer patients. The results of the gene expression analysis and survival analysis are depicted in Figures 9 a-c.

In silico molecular docking analysis

Using juglone as a target ligand for binding, *in silico* molecular docking was performed on the three primary biological targets of juglone-HDAC2, CDK2 and CDK1-identified by the network pharmacology approach. The binding energies of the interactions were determined. Juglone exhibits a strong interaction with the active centre of the HDAC2 protein, as seen in Figure 10 A-E, where a binding energy value of -7.1 kcal/mol indicates a high binding. The following amino acid residues of the target protein participated in interaction with the juglone molecule: Chain A: ASP23, ASN26, TYR27, TYR28, LYS63, ALA64, THR65, ALA66, LEU81, ARG82, SER83, ILE84, ARG85, PRO86, VAL107, PHE108, ASP109, GLY110, LEU111, PHE112, GLU113, GLN116. Chain B: TYR19, TYR59, ARG60, PRO61, HIS62, GLU68, VAL123, ALA124, VAL127, LYS128, ARG131, GLN133, GLU167. Similarly, Figure 11 A-E show different perspectives of the binding interaction between juglone and the CDK2 target protein exhibiting a binding energy value of -7.6 kcal/mol. The following amino acid residues of the target protein were involved in interaction with the juglone molecule: Chain A: ILE10, GLY11, GLY13, VAL18, ALA31, LYS33, GLU51, LEU54, LEU55, LEU58, VAL64, PHE80, GLU81, PHE82, LEU83, HIS84, GLN85, ASP86, LYS89, HIS121, ARG122, VAL123, GLN131, LEU134, ALA144, ASP145. Figure 12 A-E display diverse perspectives of the binding interaction between juglone and the CDK1 target protein exhibiting a binding energy value of only -5.6 kcal/mol indicating a weak bonding interaction of juglone with the CDK1 protein.

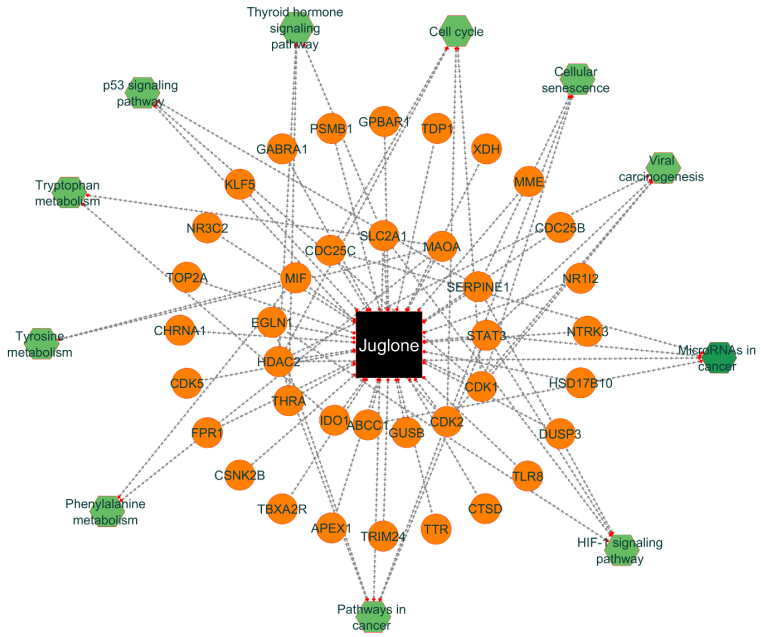

Figure 5: A detailed network exhibiting the relationship between juglone, its protein targets and the signalling pathways involved in the therapeutic effect in ovarian cancer. The network was constructed by using Cytoscape 3.10.2 software. The central red octagon shows juglone molecule, the light brown color squares represent the biological targets of juglone while as the green hexagons represent the signalling pathways involved in the therapeutic action of juglone in ovarian cancer. The network consists of 50 nodes with 74 edges with 2.96 average number of neighbors.

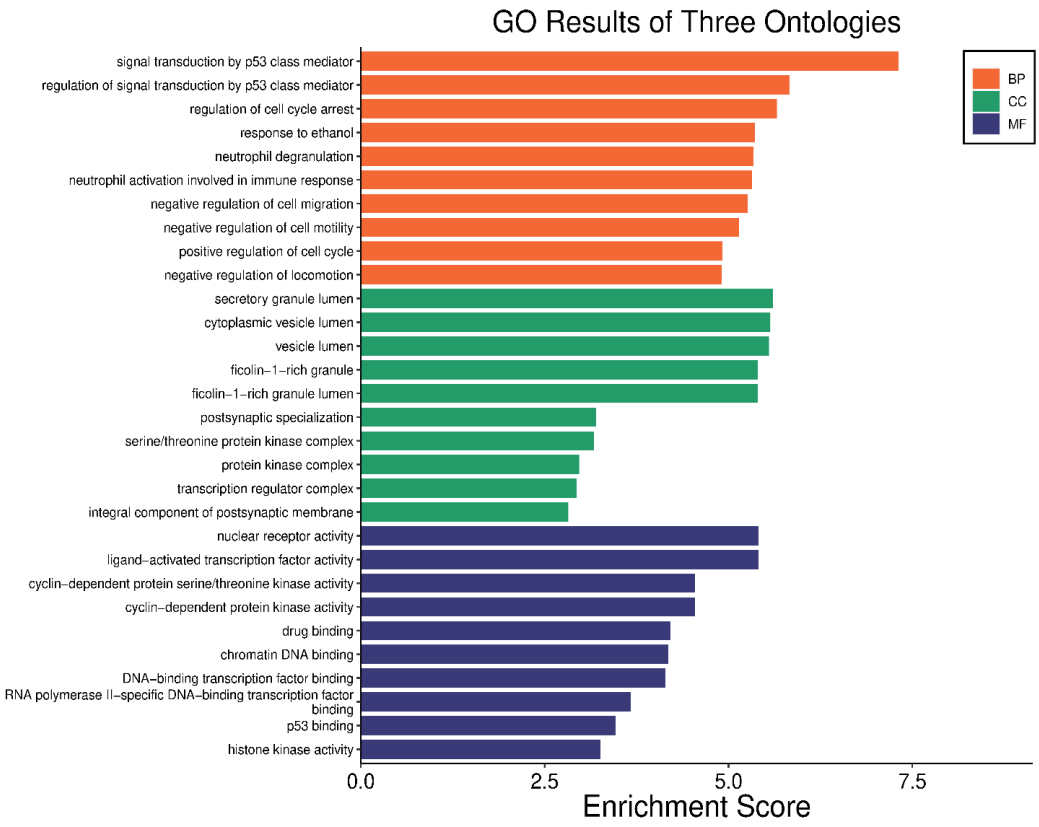

Figure 6: GO enrichment analysis of the main biological process, Molecular Function (MF) and Cellular Component (CC) connected with juglone and lung ovarian cancer. The enrichment score indicates the number of genes involved in that particular GO term.

The following amino acids were involved in the interaction: Chain A: ILE10, VAL18, ALA31, LYS33, GLU81, PHE82, LEU83, MET85, ASP86, GLN132, ASN133, LEU135, ALA145.

Experimental Validation

Juglone induced antiproliferative and apoptotic effects in OVCAR-3 human ovarian cancer cells

MTT cell viability and apoptosis assays were used to evaluate the findings of the network pharmacology and *in silico* molecular docking. The MTT experiment was carried out with varying juglone concentrations (0, 15, 30, 60 and 120 μM) and time intervals (24 and 48 hr) and the results are shown in Figure 13. The findings show that juglone inhibited the viability of OVCAR-3 human ovarian cancer cells in a concentration- and time-dependent manner. Using flow cytometry and annexin-V, the apoptosis experiment revealed that juglone molecule induced dose-dependent early and late apoptotic events in these cancer cells. Figure 14 displays the results of the apoptosis experiment, which indicate that juglone increased the percentage of early and late apoptotic cells in a dose-dependent manner.

Juglone induced G2/M phase cell cycle arrest

Effect of juglone on the cell cycle phase distribution in OVCAR-3 human cancer cells was studied by using flow cytometry using PI as a staining agent. The results are shown in Figure 15 and reveal that increasing concentrations of juglone led to a dose-dependent increase in the G2/M phase cells with a concomitant decrease in G0/G1 and S-phase cells suggesting that juglone has the tendency to induce G2/M phase cell cycle arrest in OVCAR-3 human ovarian cancer cells.

DISCUSSION

Network pharmacology and Molecular docking are indispensable bioinformatics tools in the search for anticancer drugs that work together to improve the identification and development of novel therapeutic medicines. Network pharmacology, an interdisciplinary field, powers systems biology and computational tools to understand drug actions at a systemic level. This method offers a comprehensive portrait of the pharmacological landscape by monitoring the relationships between drugs, targets and disease networks. It enables identification of multi-target drugs that can control several pathways involved in the onset and progression of cancer at the same time, increasing their efficacy and decreasing their drug resistance. Because cancer tumours are

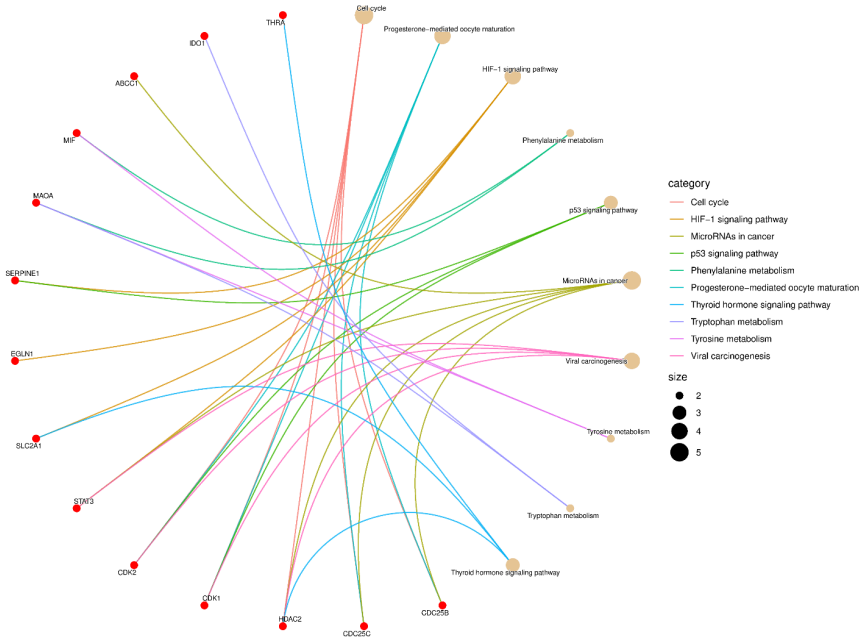

Figure 7: KEGG enrichment analysis for the identification of potential signalling pathways involved in the therapeutic targets of juglone in the treatment of ovarian cancer. The sorting of the different metabolic pathways is done based on the number of enriched genes which is indicated by size of the bubble. The bigger the bubble size, the higher the number of genes enriched in that particular pathway.

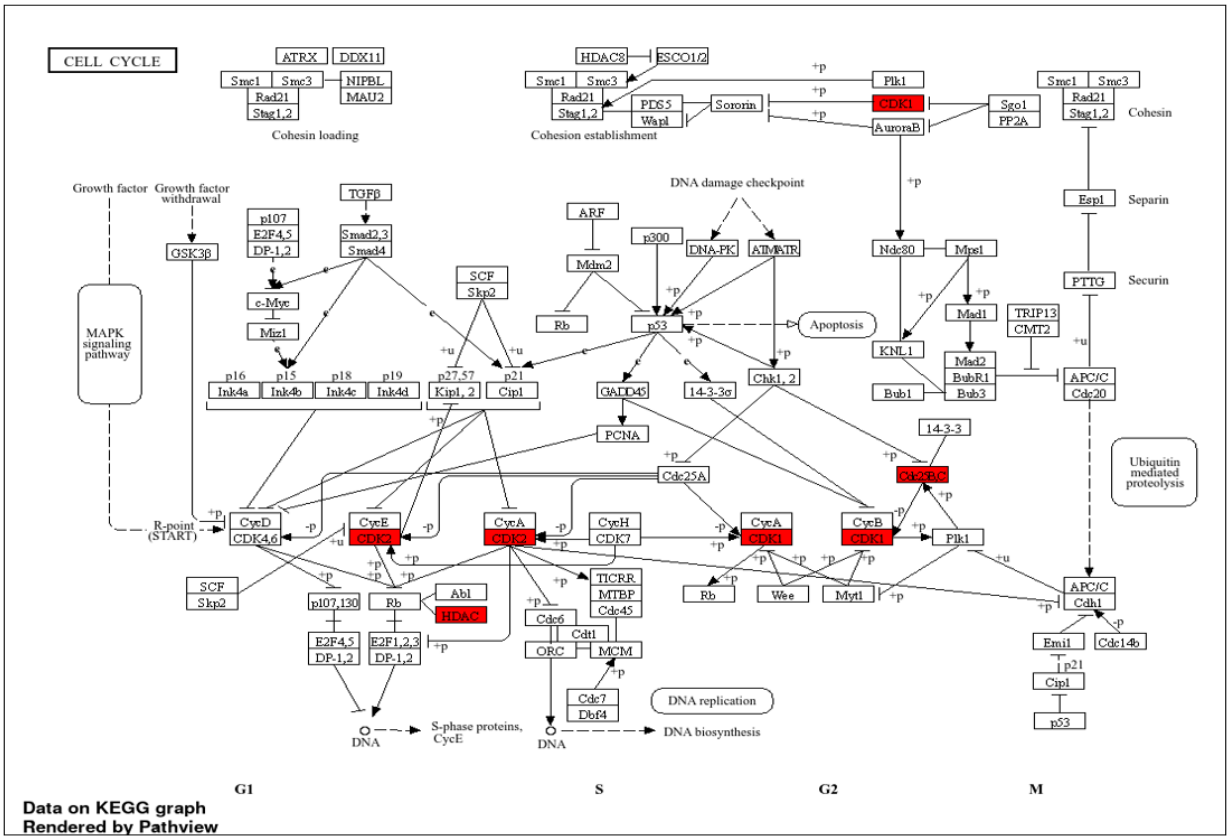

a

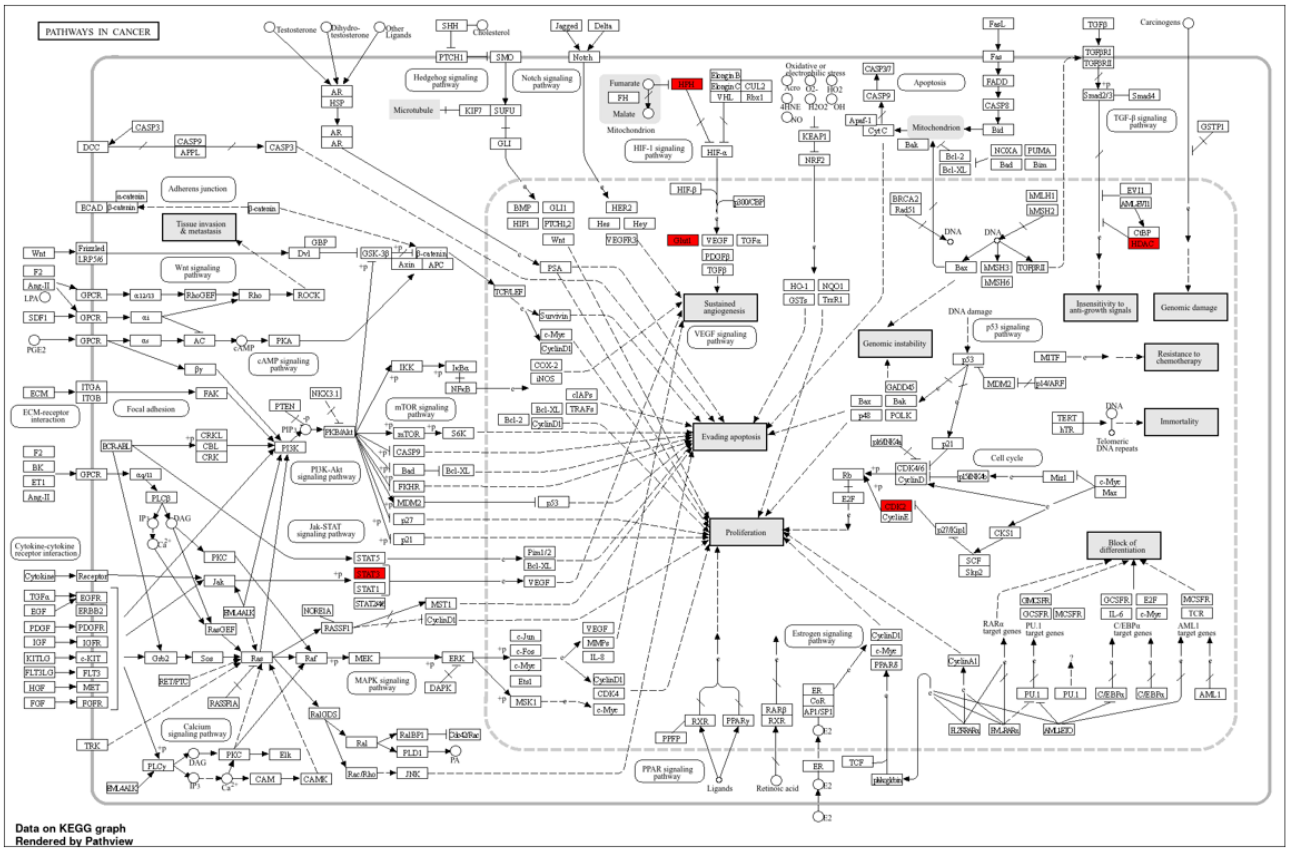

b

Figure 8: A, B: Gene mapping diagram showing two most significant signalling pathways; 8-a cell cycle and 8-b Pathways in cancer.

complex and heterogenous, a multi-target approach is essential to cancer treatment.[27,28] *In silico* molecular docking complements network pharmacology by furnishing comprehensive insights into the binding interactions between potential drugs and their biological targets. This computational procedure predicts the ideal orientation of a drug when bound to a target protein, which is crucial for understanding the mechanism of drug action. By simulating these interactions, medicinal chemists can screen huge libraries of compounds, recognize promising drug candidates and optimize their structures for better binding affinity and specificity. Docking studies have been instrumental in the discovery of numerous anticancer agents, providing critical information that guides the design and development of effective drugs.[29-31]

The combination of network pharmacology and molecular docking creates a powerful framework for anticancer drug discovery. Network pharmacology detects key nodes and pathways in cancer biology networks, highlighting potential drug targets for therapeutic intervention. Molecular docking then helps in the specific design and optimization of compounds to interact with these targets. For instance, combining these techniques has led to the identification of novel inhibitors for targets like protein kinases and proteases, which play significant roles in cancer cell proliferation and metastasis. Furthermore, these two methods are invaluable in repurposing existing drugs for new anticancer applications.[32,33]

In the current study, we used this powerful combination of network pharmacology and *in silico* molecular docking followed by experimental validation of the results. We evaluated the druglikeness, bioavailability, solubility and toxicity profile of juglone molecule using SwissADME online portal which showed that juglone has good gastrointestinal absorption and is permeable to blood brain barrier as well with a decent bioavailability score of 0.55. This allows for the further screening of this molecule by identifying its key protein targets which was performed by using Super-PRED and Swiss Target Prediction databases leading to identification of 107 targets. Using GeneCards database, 1242 disease targets (Supplementary Table S2) associated with ovarian cancer were identified. Feeding these individual targets of juglone and ovary cancer into the venny online tool led to the identification of 26 common targets between juglone and ovarian cancer. All further network analysis was performed using these common targets only because these have the highest probability of involvement in the therapeutic action

of juglone in ovarian cancer. Using the STRING database, a PPI network of these common targets was constructed identifying which protein targets exhibit connectivity among them and which are disconnected or less connected. This PPI network displays 153 edges, 26 nodes and an average node degree of 11.8. In a PPI network, target proteins are represented as nodes, while the edges show the relationships and connections between the proteins. We identified the following five hub genes using the Cyto Hubba plug-in using Cytoscape software: HDAC2 (node degree 6), CDK2 (node degree 6), CDK1 (node degree 5), STAT3 (node degree 5), MAOA (node degree 4). The pathways in cancer, the cell cycle, viral carcinogenesis and MicroRNAs in cancer were the four most important pathways found by Cyto Hubba and these pathways were directly affected by the above-mentioned hub genes. A comprehensive network showing the relationship between juglone, its biological targets and the signalling pathways it affects was also built as shown in Figure 5. The network consists of 50 nodes with 74 edges with 2.96 average number of neighbors. HDACs are implicated in many stages of cancer. Haematological and solid tumours have been connected to aberrant expression of HDACs, among other malignancies. A high level of HDACs is typically linked to advanced illness and unfavourable patient outcomes. For instance, worse outcomes in ovarian and stomach malignancies are linked to high expression of HDAC1, 2 and 3.[34,35] Cyclin-Dependent Kinases (CDKs), in particular CDK1 and CDK2, are important regulators of the cell cycle and have a major impact on the development of cancer. A number of malignancies have been related to CDK1 overexpression and using certain inhibitors to target CDK1 has showed promise in re-establishing normal cell cycle regulation and slowing tumour progression. A number of malignancies have been related to CDK1 overexpression and using certain inhibitors to target CDK1

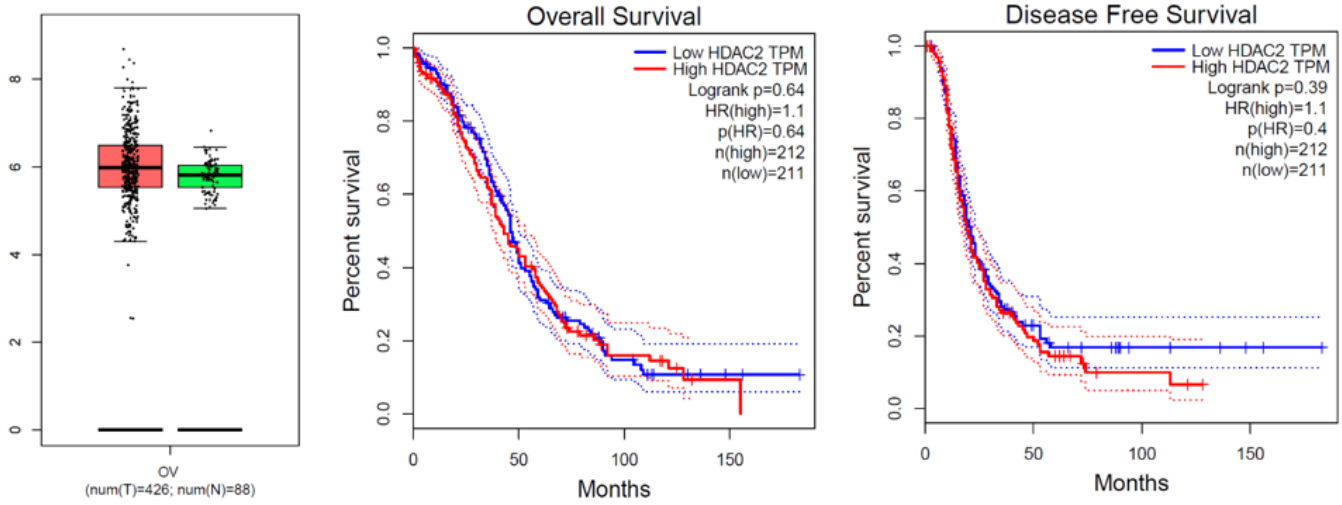

A

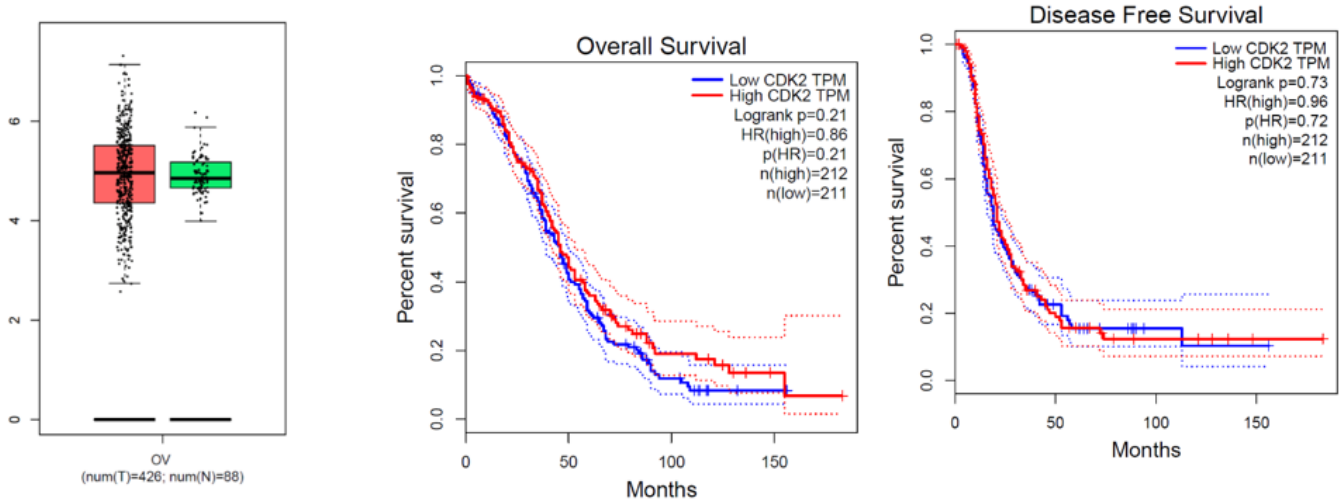

B

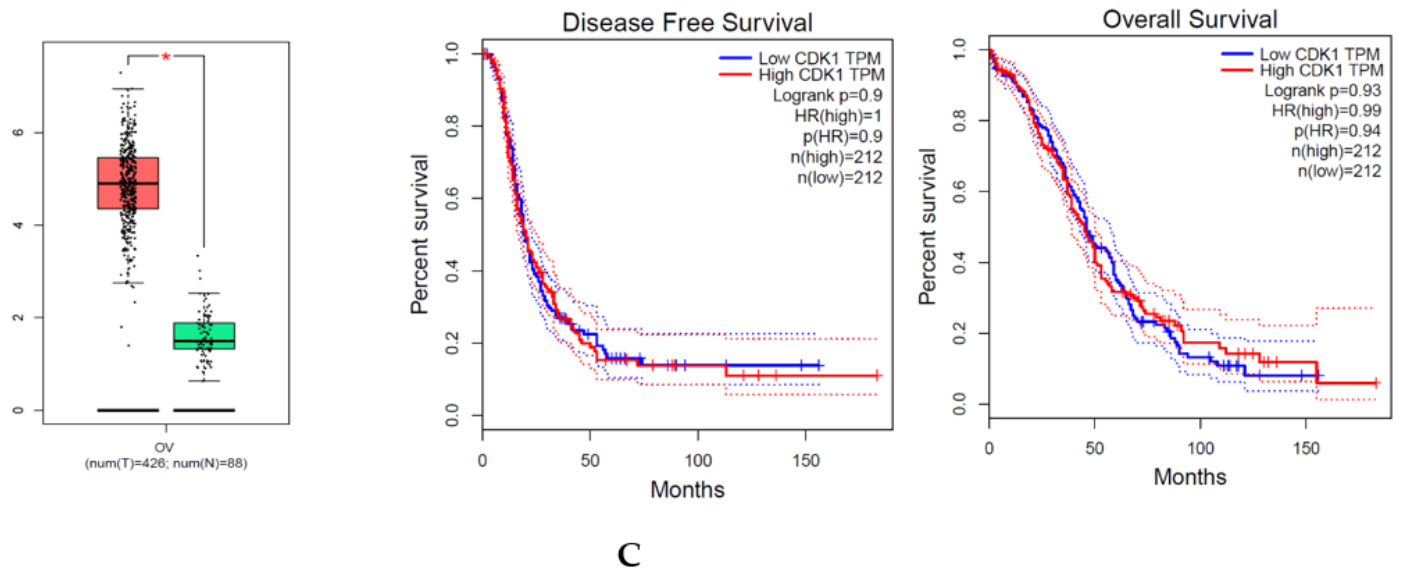

Figure 9: A-C: The gene expression level analysis and gene survival analysis of (a) HDAC2, (b) CDK2 and (c) CDK1; out of these CDK1 was highly overexpressed in ovarian cancer (n=426) compared with normal ovarian tissues (n=88), red boxes indicate tumor (T) tissues while as green boxes indicate normal (N) tissues, * p<0.05. The other survival analysis plots indicate how overexpression is associated with disease prognosis.

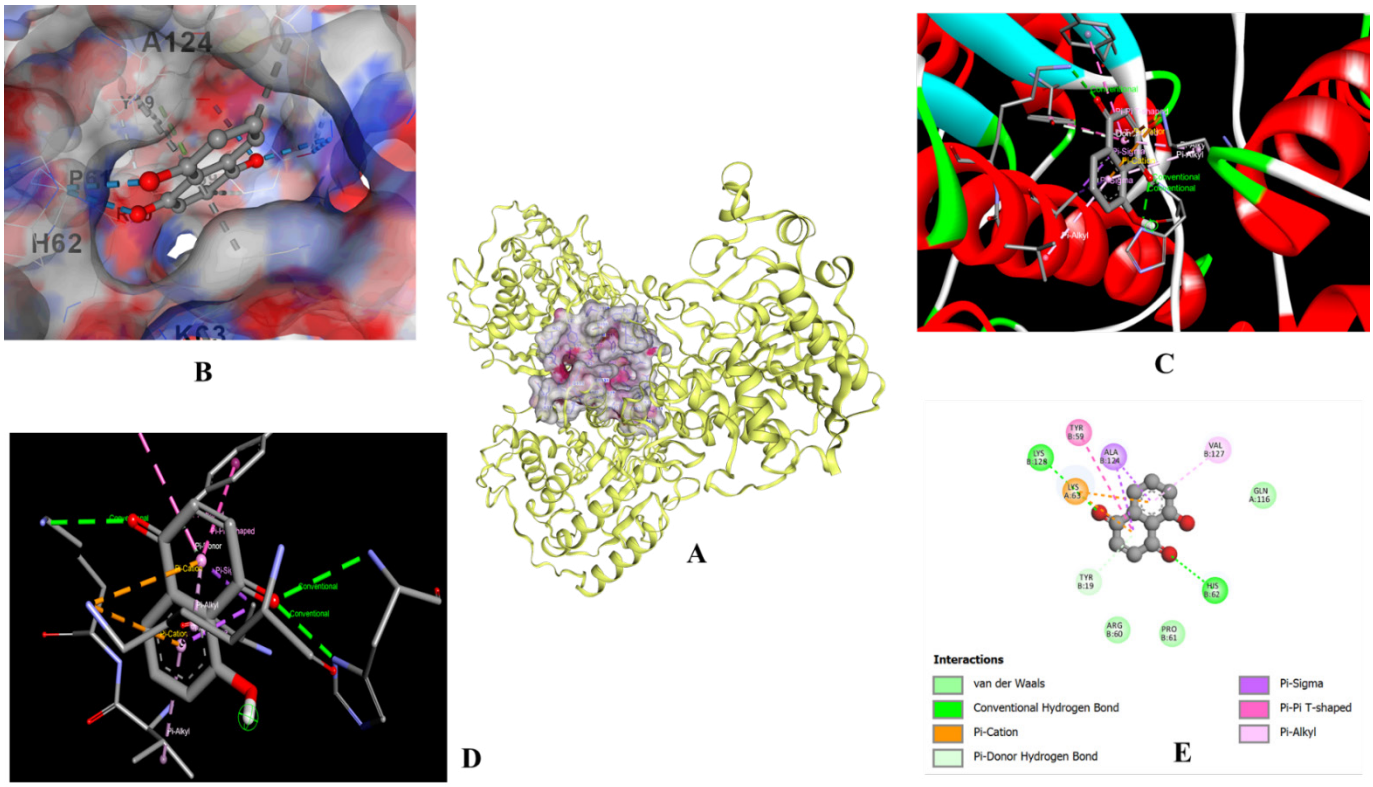

Figure 10: A-E: Figure shows various depictions of the target protein (HDAC2) along with the bound juglone ligand, A shows the cavity region of the target protein HDAC2 in ribbon model, B shows the cartoon representation of the protein surface with bound juglone molecule, C and D show 3-D while E shows 2D-representation of the target protein along with bound juglone ligand.

has shown promise in re-establishing normal cell cycle regulation and slowing tumour progression.[36,37] The GO analysis indicated that juglone participates in numerous key biological processes in ovarian cancer, including signal transduction by p53 class mediator, regulation of signal transduction by p53 class mediator, neutrophil degranulation, neutrophil activation involved in immune response, negative regulation of cell migration, negative regulation of cell motility, regulation of cell cycle arrest. The KEGG pathway analysis indicated that juglone suppresses the proliferation of ovarian cancer through various pathways, such

as cell cycle, HIF-1 signalling pathway, MicroRNAs in cancer, p53 signalling pathway, viral carcinogenesis, phenylalanine metabolism. *In silico* molecular docking analysis was performed using the three key biological targets including HDAC2, CDK2 and CDK1 and it was found that juglone exhibited strong binding affinities with HDAC2 and CDK1 and lower affinity with CDK1 as was suggested by their binding energy values which followed the order CDK2>HDAC2>CDK1. Gene expression and survival analyses using GEPIA database indicated that CDK1 gene was overexpressed in ovarian cancer tissues as compared to the normal tissues, only mild difference was seen in case of HDAC2 and CDK2 genes. Further, the overexpression of CDK1 also had a significant impact on the Overall Survival (OS) and Disease-Free Survival (DFS) of the ovarian cancer patients.

Experimental assays including the cell viability assay using MTT colorimetric dye and apoptosis assay was performed using flow cytometry and annexin-V as a staining agent. Results indicated that juglone induced significant inhibition of OVCAR-3 human ovarian cancer cell viability and these effects were mediated via induction of early and late apoptosis. The involvement of CDK2 and CDK1 in the therapeutic effect of juglone as revealed by network pharmacology encouraged us to perform cell cycle assay using flow cytometry which indicated that juglone did induce G2/M phase cell cycle arrest which actually results in cell proliferation inhibition.

Juglone exhibits potent anticancer effects across multiple tumor types by engaging diverse cellular pathways and death mechanisms. In non-small cell lung cancer, for example, juglone triggers the intrinsic apoptotic pathway through ROS generation, which leads to mitochondrial dysfunction, cytochrome-c release and caspase activation.[38] In ovarian and cervical cancer cells, it modulates the balance of pro- and anti-apoptotic proteins-upregulating Bax while downregulating Bcl-2-to promote programmed cell death.[39] In pancreatic and prostate cancer models, juglone not only induces cell cycle arrest but also interferes with survival signaling pathways such as PI3K/Akt and MAPKs, thereby enhancing apoptotic processes.[40] Additionally, juglone has been shown to inhibit metastasis by suppressing EMT markers and reducing matrix metalloproteinase expression in breast and colon cancer cells, which diminishes their invasive capabilities.[41] This multipronged action-combining ROS-mediated mitochondrial damage, modulation of apoptotic regulators, cell cycle disruption and EMT inhibition-also is consistent with our findings that juglone targets various cellular contexts and death mechanisms.

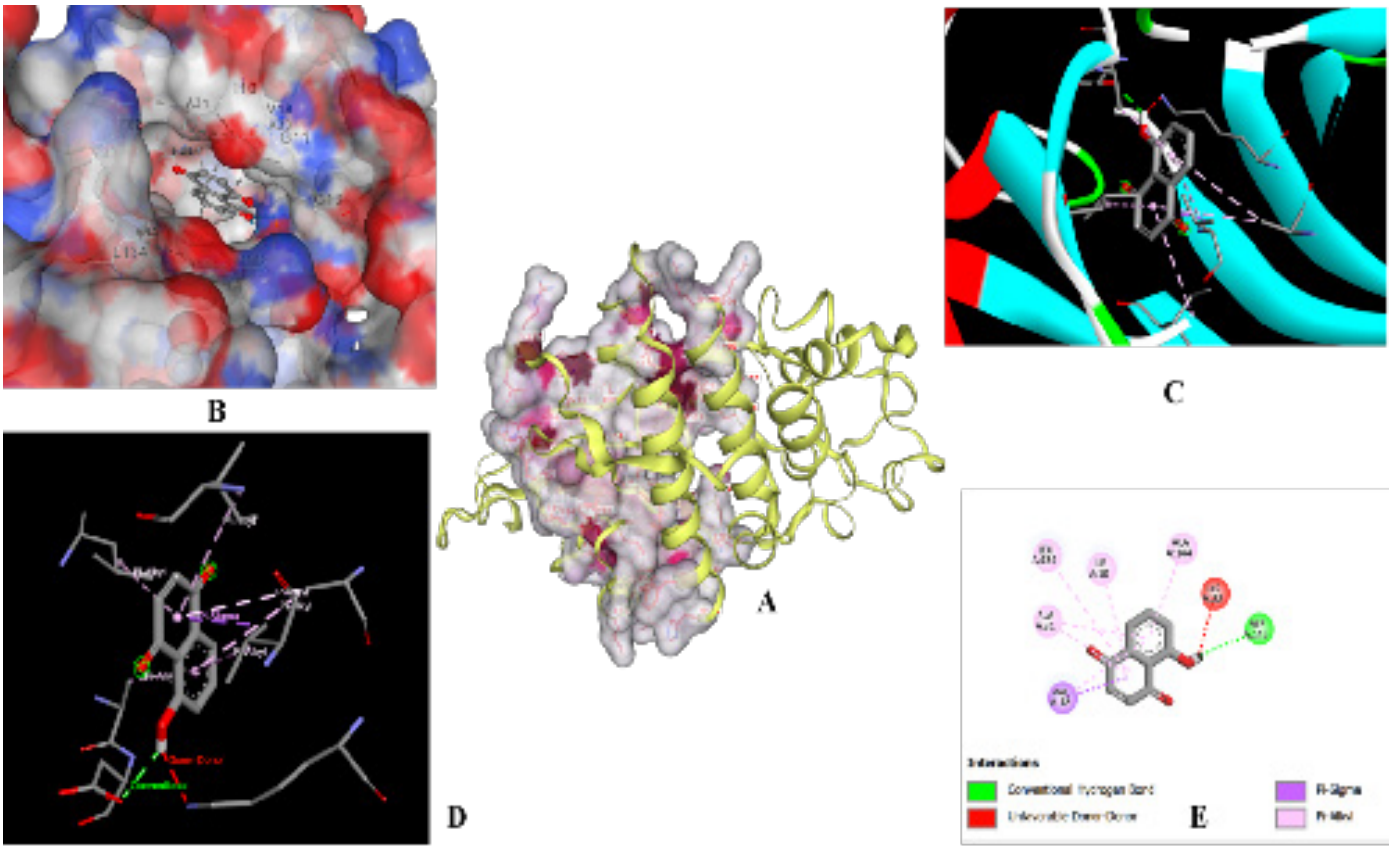

Figure 11: A-E: Figure shows various depictions of the target protein (CDK2) along with the bound juglone ligand, A shows the cavity region of the target protein CDK2 in ribbon model, B shows the cartoon representation of the protein surface with bound juglone molecule, C and D show 3-D while E shows 2D-representation of the target protein along with bound juglone ligand.

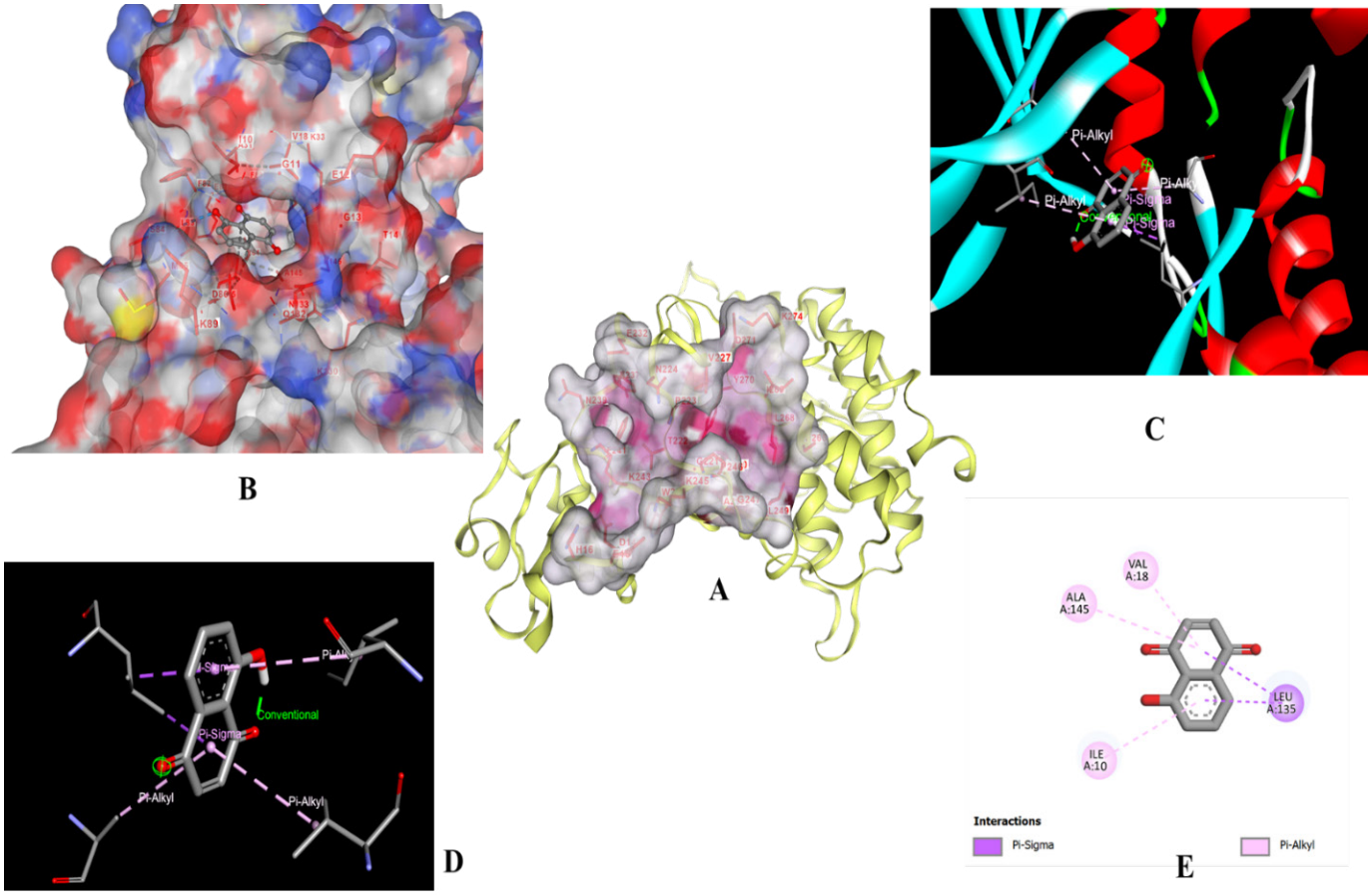

Figure 12: A-E: *In silico* molecular docking analysis depicting various representations of the target protein (CDK1) along with the bound juglone ligand, A shows the cavity site of the target protein CDK1 in ribbon model, B shows the cartoon representation of the protein surface with bound juglone molecule, C and D show 3-D while E shows 2D-representation of the target protein along with bound juglone ligand.

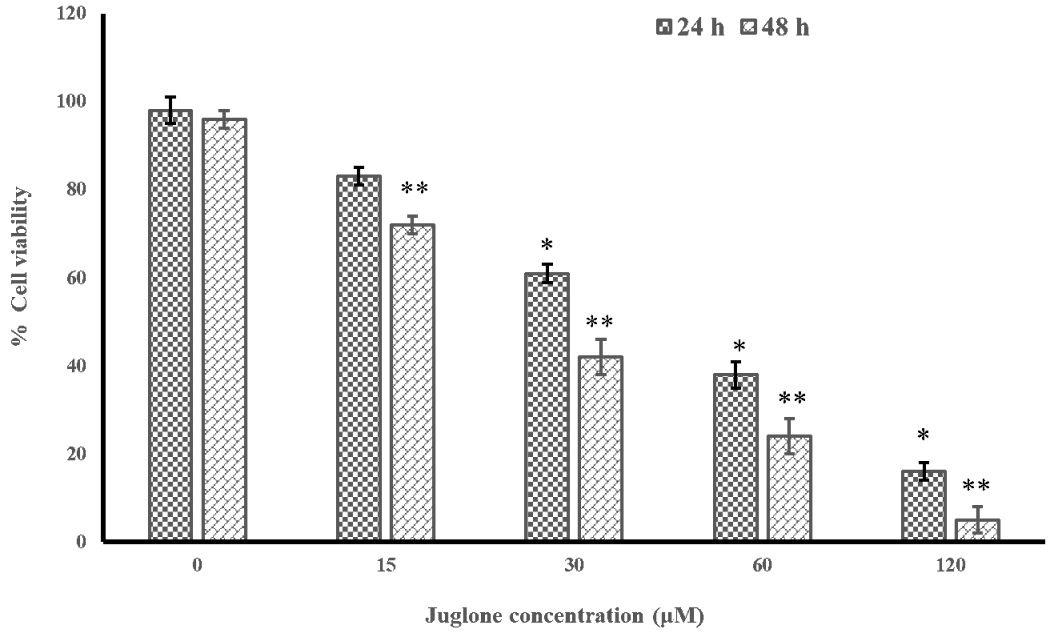

Figure 13: Results of the MTT assay demonstrating a noteworthy, dose and time-dependent suppression of cell viability brought about by increasing doses of juglone in OVCAR-3 human ovarian cancer cells. Data of individual triplicate experiments were presented as mean± SD, * $p<0.05$, ** $p<0.01$ as statistically significant with respect to the control.

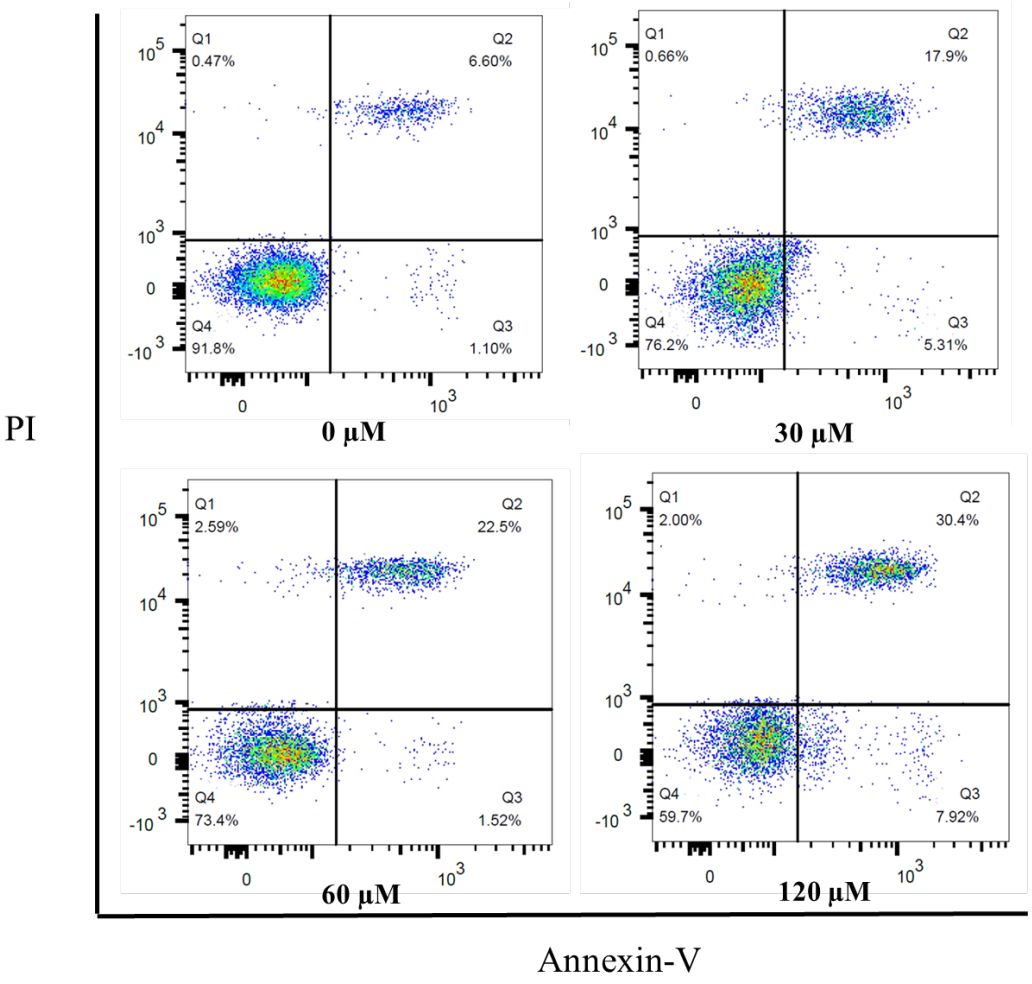

Figure 14: Annexin-V assay using flow cytometry showing the impact of increasing doses of juglone on the early and late apoptotic cell populations in OVCAR-3 human ovarian cancer cells, the results clearly show that increasing concentrations of juglone induce both early and late apoptosis in OVCAR-3 human ovarian cancer cells. The effect was much more pronounced at 120 µM dose of juglone.

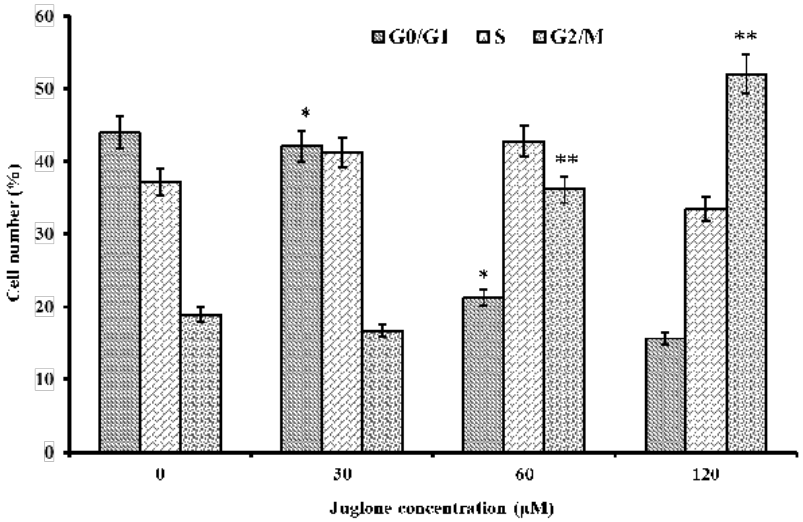

Figure 15: Cell cycle analysis by using flow cytometry technique; results indicate that increasing juglone concentrations led to a dose-dependent increase in G2/M phase cells with a concomitant decrease in G0/G1 and S phase cells indicating that juglone induced G2/M phase cell cycle arrest in OVCAR-3 human ovarian cancer cells. Data of individual triplicate experiments were shown as mean±SD, * $p<0.05$, ** $p<0.01$ as statistically significant with respect to the control.

CONCLUSION

In summary, our integrative approach combining network pharmacology, *in silico* molecular docking and experimental assays has provided evidence for the anticancer potential of juglone in human ovarian carcinoma cells. The favorable ADME profile and safety of juglone were confirmed through SwissADME and Pro-Tox 3.0 analysis. Our target prediction yielded 107 juglone targets, intersecting with 1242 ovarian cancer-related targets to produce 26 common targets, among which hub genes HDAC2, CDK2, STAT3 and CDK1 were identified. Molecular docking showed strong interactions with HDAC2 and CDK2, while GEPIA analysis revealed CDK1 overexpression correlating with poor prognosis. Experimental assays further validated concentration-dependent cytotoxic effects, induction of apoptosis and G2/M cell cycle arrest in OVCAR-3 cells for juglone. Overall, these findings highlight juglone as a promising candidate for further therapeutic development in ovarian cancer treatment.

ABBREVIATIONS

PPI: Protein-Protein Interaction; **GO:** Gene Ontology; **KEGG:** Kyoto Encyclopedia of Genes and Genomes; **FBS:** Fetal Bovine Serum; **BBB:** Blood-Brain Barrier; **GI:** Gastrointestinal Absorption; **PI:** Propidium Iodide; **HDAC2:** Histone Deacetylase 2; **MTT:** 3-(4,5-Dimethylthiazol-2-yl)-2,5-Diphenyltetrazolium Bromide (Assay); **OVCAR-3:** Human Ovarian Cancer Cell Line; **SMILE:** Simplified Molecular Input Line Entry System; **GEPIA:** Gene Expression Profiling Interactive Analysis; **STAT3:** Signal Transducer and Activator of Transcription 3; **CDK2:** Cyclin-Dependent Kinase 2; **CDK1:** Cyclin-Dependent Kinase 1; **ROS:** Reactive Oxygen Species; **RPMI:** Roswell Park Memorial Institute (Medium); **FITC:** Fluorescein Isothiocyanate; **SEM:** Standard Error of Mean; **ANOVA:** Analysis of Variance.

CONFLICT OF INTEREST

The authors declare that there is no conflict of interest.

SUMMARY

In summary, the SwissADME analysis revealed favorable pharmacokinetics for juglone, including high GI absorption and rare BBB permeability, with a bioavailability score of 0.55. Pro-Tox 3.0 indicated no significant toxicity, suggesting juglone's safe profile. Target prediction identified 107 juglone targets, while ovarian cancer target analysis revealed 1,242 disease-related targets. Using the Venny tool, 26 common targets between juglone and ovarian cancer were identified, representing key points of therapeutic interaction.

The PPI network highlighted five hub genes: HDAC2, CDK2, CDK1, STAT3 and MAOA, associated with critical pathways like cell cycle regulation and cancer progression. The GO and KEGG enrichment analysis linked the activity of juglone to key biological processes (e.g., cell cycle arrest, signal transduction) and pathways (e.g., p53 signaling, HIF-1 signaling, MicroRNAs in cancer). *In silico* molecular docking confirmed strong binding interactions of juglone with HDAC2 (-7.1 kcal/mol) and CDK2 (-7.6 kcal/mol), while its binding to CDK1 (-5.6 kcal/mol) was weaker. Experimental validation showed concentration- and time-dependent cytotoxic effects of juglone, apoptosis induction and G2/M phase cell cycle arrest in OVCAR-3 cells. Overall, juglone demonstrates promising anticancer potential through its interaction with key molecular targets and pathways, supporting its therapeutic role in ovarian cancer.

REFERENCES

1. Chandra A, Pius C, Nabeel M, Nair M, Vishwanatha JK, Ahmad S, *et al.* Ovarian cancer: current status and strategies for improving therapeutic outcomes. Cancer Med. 2019; 8(16): 7018-31. doi: 10.1002/cam4.2560, PMID 31560828.
2. Bayram D, Armagan İ, Özgöcmen M, Senol N, Calapoglu M. Determination of apoptotic effect of juglone on human bladder cancer TCC-SUP and RT-4 cells: an *in vitro* study. J Environ Pathol Toxicol Oncol. 2018; 37(2): 173-81. doi: 10.1615/JEnvironPatholToxicolOncol.2018025226, PMID 30055552.
3. Jin X, Zhang Y, Zhang Z, Che D, Lv H. Juglone loaded Poloxamer 188/phospholipid mixed micelles evaluated *in vitro* and *in vivo* in breast cancer. Int J Pharm. 2016; 515(1-2): 359-66. doi: 10.1016/j.ijpharm.2016.10.027, PMID 27744033.
4. Pavan V, Ribaudo G, Zorzan M, Redaelli M, Pezzani R, Mucignat-Caretta C, *et al.* Antiproliferative activity of juglone derivatives on rat glioma. Nat Prod Res. 2017; 31(6): 632-8. doi: 10.1080/14786419.2016.1214830, PMID 27465779.
5. Zhang XB, Zou CL, Duan YX, Wu F, Li G. Activity guided isolation and modification of juglone from Juglans regia as potent cytotoxic agent against lung cancer cell lines. BMC Complement Altern Med. 2015; 15: 396. doi: 10.1186/s12906-015-0920-0, PMID 26530090.
6. Wang P, Zhang SD, Jiao J, Wang W, Yu L, Zhao XL, *et al.* ROS-mediated p53 activation by juglone enhances apoptosis and autophagy *in vivo* and *in vitro*. Toxicol Appl Pharmacol. 2019; 379: 114647. doi: 10.1016/j.taap.2019.114647, PMID 31283929.
7. Zhang J, Fu M, Wu J, Fan F, Zhang X, Li C, *et al.* The anti-glioma effect of juglone derivatives through ROS generation. Front Pharmacol. 2022; 13: 911760. doi: 10.3389/fphar.2022.911760, PMID 35774612.
8. Zhong J, Hua Y, Zou S, Wang B. Juglone triggers apoptosis of non-small cell lung cancer through the reactive oxygen species-mediated PI3K/Akt pathway. PLOS One. 2024; 19(5): e0299921. doi: 10.1371/journal.pone.0299921, PMID 38814975.
9. Wang P, Gao C, Wang W, Yao LP, Zhang J, Zhang SD, *et al.* Juglone induces apoptosis and autophagy via modulation of mitogen-activated protein kinase pathways in human hepatocellular carcinoma cells. Food Chem Toxicol. 2018; 116(B):40-50. doi: 10.1016/j.fct.2018.04.004, PMID 29627502.
10. Zhang YY, Zhang F, Zhang YS, Thakur K, Zhang JG, Liu Y, *et al.* Mechanism of juglone-induced cell cycle arrest and apoptosis in Ishikawa human endometrial cancer cells. J Agric Food Chem. 2019; 67(26): 7378-89. doi: 10.1021/acs.jafc.9b02759, PMID 31184118.
11. Hopkins AL. Network pharmacology: the next paradigm in drug discovery. Nat Chem Biol. 2008; 4(11): 682-90. doi: 10.1038/nchembio.118, PMID 18936753.
12. Yildirim MA, Goh KI, Cusick ME, Barabási AL, Vidal M. Drug-target network. Nat Biotechnol. 2007; 25(10): 1119-26. doi: 10.1038/nbt1338, PMID 17921997.
13. Cheng F, Liu C, Jiang J, Lu W, Li W, Liu G, *et al.* Prediction of drug-target interactions and drug repositioning via network-based inference. PLOS Comput Biol. 2012; 8(5): e1002503. doi: 10.1371/journal.pcbi.1002503, PMID 22589709.
14. Shang L, Wang Y, Li J, Zhou F, Xiao K, Liu Y, *et al.* Mechanism of Sijunzi Decoction in the treatment of colorectal cancer based on network pharmacology and experimental validation. J Ethnopharmacol. 2023; 302(A):115876. doi: 10.1016/j.jep.2022.115876, PMID 36343798.
15. Yuan C, Wang MH, Wang F, Chen PY, Ke XG, Yu B, *et al.* Network pharmacology and molecular docking reveal the mechanism of scopoletin against non-small cell lung cancer. Life Sci. 2021; 270: 119105. doi: 10.1016/j.lfs.2021.119105, PMID 33497736.
16. He Q, Liu C, Wang X, Rong K, Zhu M, Duan L, *et al.* Exploring the mechanism of curcumin in the treatment of colon cancer based on network pharmacology and molecular docking. Front Pharmacol. 2023; 14: 1102581. doi: 10.3389/fphar.2023.1102581, PMID 36874006.
17. Daina A, Michielin O, Zoete V. SwissADME: a free web tool to evaluate pharmacokinetics, drug-likeness and medicinal chemistry friendliness of small molecules. Sci Rep. 2017; 7(1): 42717. doi: 10.1038/srep42717, PMID 28256516.
18. Daina A, Michielin O, Zoete V. SwissTargetPrediction. SwissTargetPrediction: updated data and new features for efficient prediction of protein targets of small molecules. Nucleic Acids Res. 2019; 47(W1):W357-64. doi: 10.1093/nar/gkz382, PMID 31106366.

19. Gallo K, Goede A, Preissner R, Gohlke BO. SuperPred 3.0: drug classification and target prediction-a machine learning approach. Nucleic Acids Res. 2022; 50(W1):W726-31. doi: 10.1093/nar/gkac297, PMID 35524552.
20. WUniProt Consortium. UniProt: the universal protein knowledgebase in 2025. Nucleic Acids Res. 2025; 53(D1):D609-17. doi: 10.1093/nar/gkae1010, PMID 39552041.
21. Stelzer G, Rosen N, Plaschkes I, Zimmerman S, Twik M, Fishilevich S, *et al.* The GeneCards suite: from gene data mining to disease genome sequence analyses. Curr Protoc Bioinformatics. 2016; 54(1): 1.30.1-1.30.33. doi: 10.1002/cpbi.5, PMID 27322403.
22. Szklarczyk D, Kirsch R, Koutrouli M, Nastou K, Mehryary F, Hachilif R, *et al.* The STRING database in 2023: protein-protein association networks and functional enrichment analyses for any sequenced genome of interest. Nucleic Acids Res. 2023; 51(D1):D638-46. doi: 10.1093/nar/gkac1000, PMID 36370105.
23. Liu Y, Yang X, Gan J, Chen S, Xiao ZX, Cao Y. CB-Dock2: improved protein-ligand blind docking by integrating cavity detection, docking and homologous template fitting. Nucleic Acids Res. 2022; 50(W1):W159-64. doi: 10.1093/nar/gkac394, PMID 35609983.
24. Liu Y, Grimm M, Dai WT, Hou MC, Xiao ZX, Cao Y. CB-Dock: A web server for cavity detection-guided protein-ligand blind docking. Acta Pharmacol Sin. 2020; 41(1): 138-44. doi: 10.1038/s41401-019-0228-6, PMID 31263275.
25. Tang Z, Li C, Kang B, Gao G, Li C, Zhang Z. Gepia: a web server for cancer and normal gene expression profiling and interactive analyses. Nucleic Acids Res. 2017; 45(W1):W98-W102. doi: 10.1093/nar/gkx247, PMID 28407145.
26. Stelzer G, Rosen N, Plaschkes I, Zimmerman S, Twik M, Fishilevich S, *et al.* The GeneCards suite: from gene data mining to disease genome sequence analyses. Curr Protoc Bioinformatics. 2016; 54: 1.30.1-1.30.33. doi: 10.1002/cpbi.5, PMID 27322403.
27. Wang X, Wang ZY, Zheng JH, Li S. TCM network pharmacology: a new trend towards combining computational, experimental and clinical approaches. Chin J Nat Med. 2021; 19(1): 1. doi: 10.1016/S1875-5364(21)60001-8, PMID 33516447.
28. Wu Z, Zhu Z, Cao J, Wu W, Deng C, Xie Q, *et al.* Prediction of network pharmacology, molecular docking-based strategy and vitro assays to determine potential pharmacological mechanism of Dioscoreae bulbiferae and Bruceae fructus against laryngocarcinoma. Medicine. 2023; 102(51): e36771. doi: 10.1097/MD.0000000000036771, PMID 38134081.
29. Pagadala NS, Syed K, Tuszynski J. Software for molecular docking: a review. Biophys Rev. 2017; 9(2): 91-102. doi: 10.1007/s12551-016-0247-1, PMID 28510083.
30. Kitchen DB, Decornez H, Furr JR, Bajorath J. Docking and scoring in virtual screening for drug discovery: methods and applications. Nat Rev Drug Discov. 2004; 3(11): 935-49. doi: 10.1038/nrd1549, PMID 15520816.
31. Meng XY, Zhang HX, Mezei M, Cui M. Molecular docking: a powerful approach for structure-based drug discovery. Curr Comput Aided Drug Des. 2011; 7(2): 146-57. doi: 10.2174/157340911795677602, PMID 21534921.
32. Barabási AL, Gulbahce N, Loscalzo J. Network medicine: a network-based approach to human disease. Nat Rev Genet. 2011; 12(1): 56-68. doi: 10.1038/nrg2918, PMID 21164525.
33. Lotfi Shahreza M, Ghadiri N, Mousavi SR, Varshosaz J, Green JR. A review of network-based approaches to drug repositioning. Brief Bioinform. 2018; 19(5): 878-92. doi: 10.1093/bib/bbx017, PMID 28334136.
34. Sudo T, Mimori K, Nishida N, Kogo R, Iwaya T, Tanaka F, *et al.* Histone deacetylase 1 expression in gastric cancer. Oncol Rep. 2011; 26(4): 777-82. doi: 10.3892/or.2011.1361, PMID 21725604.
35. Weichert W, Denkert C, Noske A, Darb-Esfahani S, Dietel M, Kalloger SE, *et al.* Expression of class I histone deacetylases indicates poor prognosis in endometrioid subtypes of ovarian and endometrial carcinomas. Neoplasia. 2008; 10(9): 1021-7. doi: 10.1593/neo.08474, PMID 18714364.
36. Sofi S, Mehraj U, Qayoom H, Aisha S, Almilaibary A, Alkhanani M, *et al.* Targeting cyclin-dependent kinase 1 (CDK1) in cancer: molecular docking and dynamic simulations of potential CDK1 inhibitors. Med Oncol. 2022; 39(9): 133. doi: 10.1007/s12032-022-01748-2, PMID 35723742.
37. He F, Wang X, Wu Q, Liu S, Cao Y, Guo X, *et al.* Identification of potential ATP-competitive cyclin-dependent kinase 1 inhibitors: de novo drug generation, molecular docking and molecular dynamics simulation. Comput Biol Med. 2023; 155: 106645. doi: 10.1016/j.compbiomed.2023.106645, PMID 36774892.
38. Zhong J, Hua Y, Zou S, Wang B. Juglone triggers apoptosis of non-small cell lung cancer through the reactive oxygen species-mediated PI3K/Akt pathway. PLOS One. 2024; 19(5): e0299921. doi: 10.1371/journal.pone.0299921, PMID 38814975.
39. Ahmad T, Suzuki YJ. Juglone in oxidative stress and cell signaling. Antioxidants (Basel). 2019; 8(4): 91. doi: 10.3390/antiox8040091, PMID 30959841.
40. Kaya DE, Dursunoğlu D. The anticancer activity of juglone via inducing programmed cell death in pancreatic cancer cells. Selçuk Sağlık Derg. 2023; 4(2): 321-32.
41. Zou C, Yu Y, Wang H, Matunda C, Ding S, Wang L, *et al.* Juglone inhibits tumor metastasis by regulating stemness characteristics and the epithelial-to-mesenchymal transition in cancer cells both *in vitro* and *in vivo*. Front Biosci (Landmark Ed). 2023; 28(2): 26. doi: 10.31083/j.fbl2802026, PMID 36866547.

Cite this article: Wu M, Xia Q, Liu L, Kang L. Anticancer and Apoptotic Effects of Juglone in Ovarian Carcinoma: An Integrated Computational and Experimental Study. Indian J of Pharmaceutical Education and Research. 2026;60(3):1096-112.

Supplementary Table S1: Identified Targets of juglone molecule using SuperPred and SwissTargetPrediction databases.

Target Name	ChEMBL-ID	UniProt ID	PDB Visualization	Probability
Tyrosyl-DNA phosphodiesterase 1	CHEMBL1075138	Q9NUW8	6N0D	100%
Indoleamine 2,3-dioxygenase		P14902		73%
Dual specificity phosphatase Cdc25B		P30305		73%
Endoplasmic reticulum-associated amyloid beta-peptide-binding protein	CHEMBL4159	Q99714	2O23	100%
Cathepsin D	CHEMBL2581	P07339	4OD9	95.48%
Transcription intermediary factor 1-alpha	CHEMBL3108638	O15164	4YBM	94.60%
Monoamine oxidase A	CHEMBL1951	P21397	2Z5Y	94.48%
Dual specificity phosphatase Cdc25C	CHEMBL2378	P30307	3OP3	89.60%
DNA-(apurinic or apyrimidinic site) lyase	CHEMBL5619	P27695	6BOW	87.66%
Casein kinase II alpha/beta	CHEMBL3038477	P67870	6TLS	85.65%
Thyroid hormone receptor alpha	CHEMBL1860	P10827	3ILZ	85.33%
Cyclin-dependent kinase 5/CDK5 activator 1	CHEMBL1907600	Q00535	1UNL	84.54%
Dual specificity phosphatase Cdc25B	CHEMBL4804	P30305	1QB0	84.13%
Signal transducer and activator of transcription 3	CHEMBL4026	P40763	6QHD	82.63%
Glucose transporter	CHEMBL2535	P11166	6THA	82.28%
Histone deacetylase 2	CHEMBL1937	Q92769	7KBG	82.02%
Cyclin-dependent kinase 5	CHEMBL4036	Q00535	4AU8	81.83%
DNA topoisomerase II alpha	CHEMBL1806	P11388	6ZY5	80.22%
Kruppel-like factor 5	CHEMBL1293249	Q13887	Not Available	77.64%
Egl nine homolog 1	CHEMBL5697	Q9GZT9	4BQY	77.37%
Proteasome component C5	CHEMBL4208	P20618	6KWY	75.24%
Xanthine dehydrogenase	CHEMBL1929	P47989	2E1Q	73.73%
Pregnane X receptor	CHEMBL3401	O75469	6TFI	72.74%
Dual specificity protein phosphatase 3	CHEMBL2635	P51452	3F81	72.45%
Transthyretin	CHEMBL3194	P02766	6SUG	70.84%
Cyclin-dependent kinase 1/cyclin B	CHEMBL2094127	P06493	6GU2	70%
Beta-glucuronidase	CHEMBL2728	P08236	3HN3	69.27%
Macrophage migration inhibitory factor	CHEMBL2085	P14174	6B1K	67.84%
Thromboxane A2 receptor	CHEMBL2069	P21731	Not Available	67.17%
Formyl peptide receptor 1	CHEMBL3359	P21462	Not Available	67.09%
Acetylcholine receptor; alpha1/beta1/delta/gamma	CHEMBL1907588	P02708	5HBT	66.74%
Mineralocorticoid receptor	CHEMBL1994	P08235	4PF3	66.24%
GABA-A receptor; alpha-1/beta-2/gamma-2	CHEMBL2095172	P14867	6X3T	66.19%
G-protein coupled bile acid receptor 1	CHEMBL5409	Q8TDU6	7CFM	65.89%
Multidrug resistance-associated protein 1	CHEMBL3004	P33527	4C3Z	65.77%
Neprilysin	CHEMBL1944	P08473	6SUK	65.69%
Cyclin-dependent kinase 1	CHEMBL308	P06493	6GU2	65.64%
Plasminogen activator inhibitor-1	CHEMBL3475	P05121	3CVM	65.37%
Cyclin-dependent kinase 2	CHEMBL301	P24941	5LMK	65.21%
NT-3 growth factor receptor	CHEMBL5608	Q16288	6KZD	65.07%

Target Name	ChEMBL-ID	UniProt ID	PDB Visualization	Probability
Toll-like receptor 8	CHEMBL5805	Q9NR97	3WN4	65.05%
Histone deacetylase 8	CHEMBL3192	Q9BY41	5VI6	64.99%
Nuclear receptor ROR-beta	CHEMBL3091268	Q92753	Not Available	64.70%
Glycine transporter 2	CHEMBL3060	Q9Y345	Not Available	63.13%
Dipeptidyl peptidase IX	CHEMBL4793	Q86TI2	6EOR	63.10%
G protein-coupled receptor kinase 5	CHEMBL5678	P34947	4TND	63.09%
Serine/threonine-protein kinase MST2	CHEMBL4708	Q13188	6AO5	62.61%
Nuclear factor NF-kappa-B p105 subunit	CHEMBL3251	P19838	1SVC	62.53%
Coagulation factor XIII	CHEMBL4530	P00488	4KTY	62.25%
Aminopeptidase N	CHEMBL1907	P15144	4FYT	62%
Dopamine D1 receptor	CHEMBL2056	P21728	7JVP	61.99%
Glycine receptor subunit alpha-1	CHEMBL5845	P23415	4X5T	61.42%
Lysosomal Pro-X carboxypeptidase	CHEMBL2335	P42785	3N2Z	60.98%
Prostanoid EP1 receptor	CHEMBL1811	P34995	Not Available	60.96%
Proteasome Macropain subunit	CHEMBL3492	P49721	5LE5	60.82%
Serotonin 3a (5-HT3a) receptor	CHEMBL1899	P46098	Not Available	60.56%
BMP-2-inducible protein kinase	CHEMBL4522	Q9NSY1	4W9W	60.10%
Neuronal acetylcholine receptor; alpha4/beta4	CHEMBL1907591	P30926	6UR8	59.97%
MAP/microtubule affinity-regulating kinase 4	CHEMBL5754	Q96L34	5ES1	59.95%
CDK2/Cyclin A	CHEMBL3038469	P24941	4BCN	59.83%
Protein Mdm4	CHEMBL1255126	O15151	6Q9Y	59.71%
DNA topoisomerase I	CHEMBL1781	P11387	1K4T	59.65%
ADAM10	CHEMBL5028	O14672	6BE6	58.93%
Mitogen-activated protein kinase kinase kinase 11	CHEMBL2708	Q16584	5K26	58.74%
Integrin alpha-5/beta-1	CHEMBL2095226	P05556	7NWL	58.59%
Platelet-derived growth factor receptor alpha	CHEMBL2007	P16234	7LBF	58.30%
Ribosomal protein S6 kinase alpha 1	CHEMBL2553	Q15418	2Z7Q	58.10%
Tissue factor pathway inhibitor	CHEMBL3713062	P10646	5NMV	57.98%
Cyclin-dependent kinase 1/cyclin B1	CHEMBL1907602	P06493	6GU2	57.88%
Arachidonate 12-lipoxygenase	CHEMBL3687	P18054	3D3L	57.87%
Methionine aminopeptidase 2	CHEMBL3922	P50579	1B6A	56.94%
Nuclear factor erythroid 2-related factor 2	CHEMBL1075094	Q16236	2FLU	56.71%
Beta-glucosidase	CHEMBL3761	Q9HCG7	Not Available	56.39%
Cytochrome P450 3A4	CHEMBL340	P08684	5VCC	56.25%
Free fatty acid receptor 1	CHEMBL4422	O14842	5TZR	56.22%
Muscarinic acetylcholine receptor M4	CHEMBL1821	P08173	5DSG	56.10%
Galectin-3	CHEMBL4531	P17931	6FOF	56.01%
Calpain 1	CHEMBL3891	P07384	1ZCM	55.94%
Glucocorticoid receptor	CHEMBL2034	P04150	4UDD	55.36%
Glutaminase kidney isoform, mitochondrial	CHEMBL2146302	O94925	3UO9	55.13%
Glutathione S-transferase Pi	CHEMBL3902	P09211	5J41	54.82%
Cyclin-dependent kinase 2/cyclin E1	CHEMBL1907605	P24864	1W98	54.36%

Target Name	ChEMBL-ID	UniProt ID	PDB Visualization	Probability
Angiotensin-converting enzyme	CHEMBL1808	P12821	5AMB	54.03%
Muscarinic acetylcholine receptor M1	CHEMBL216	P11229	6OIJ	54.02%
Proteinase-activated receptor 1	CHEMBL3974	P25116	3VW7	53.73%
IgG receptor FcRn large subunit p51	CHEMBL5966	P55899	6FGB	53.44%
Dipeptidyl peptidase VIII	CHEMBL4657	Q6V1X1	6EOP	53.09%
Endoplasmic reticulum aminopeptidase 1	CHEMBL5939	Q9NZ08	6Q4R	53.04%
Histone deacetylase 10	CHEMBL5103	Q969S8	Not Available	52.73%
Growth factor receptor-bound protein 2	CHEMBL3663	P62993	1GRI	52.40%
Tyrosine- and threonine-specific cdc2-inhibitory kinase	CHEMBL3984	Q99640	5VCZ	52.22%
LSD1/CoREST complex	CHEMBL3137262	O60341	5L3D	52.13%
Pyroglutamylated RFamide peptide receptor	CHEMBL5852	Q96P65	Not Available	51.85%
Dual specificity protein kinase CLK4	CHEMBL4203	Q9HAZ1	6FYV	51.79%
Eukaryotic translation initiation factor 2-alpha kinase 1	CHEMBL6029	Q9BQI3	Not Available	51.77%
Adaptor-associated kinase	CHEMBL3830	Q2M2I8	5TE0	51.68%
Ribosomal protein S6 kinase alpha 6	CHEMBL4924	Q9UK32	6G77	51.66%
Phosphodiesterase 11A	CHEMBL2717	Q9HCR9	Not Available	51.57%
DCN1-like protein 1	CHEMBL4105838	Q96GG9	6BG3	51.35%
Peptidyl-prolyl cis-trans isomerase NIMA-interacting 1	CHEMBL2288	Q13526	1PIN	51.01%
AMP-activated protein kinase, alpha-1 subunit	CHEMBL4045	Q13131	6C9H	51%
Vasopressin V1b receptor	CHEMBL1921	P47901	Not Available	50.53%
Sodium channel protein type III alpha subunit	CHEMBL5163	Q9NY46	Not Available	50.46%
E3 SUMO-protein ligase CBX4	CHEMBL3232685	O00257	5EPL	50.23%
Excitatory amino acid transporter 1	CHEMBL3085	P43003	5LM4	50.22%
Vascular endothelial growth factor receptor 1	CHEMBL1868	P17948	5T89	50.21%
SUMO-activating enzyme	CHEMBL2095174	Q9UBE0	6XOG	50.16%

Supplementary Table S2: Identified Targets of Ovarian cancer using GeneCards database.

BRCA1
BRCA2
TP53
ATM
MSH6
CDH1
BRIP1
MSH2
CHEK2
MLH1
APC
PMS2
BARD1
PTEN
EGFR
POLE
NBN
RAD50
PIK3CA
DICER1
CDKN2A
NF1
ERBB2
KRAS
AXIN2
BRAF
BLM
RET
MET
TSC2
CTNNB1
ALK
MRE11
PTCH1
RB1
AKT1
STK11
SMAD4
KIT
BMPR1A
AR
TSC1
SMARCA4
FANCC
CDKN1B
TERT
PDGFRA
CTNNA1
FH
ESR1
EPCAM
HRAS
BAP1
CDK4
WT1
ERCC2
FGFR2
FANCD2
SMARCB1
CCND1
RAD51
MTOR
MYC
SDHA
FANCA
BUB1B
FGFR3
PRKN
VHL
WRN
FSHR
ERBB3
NRAS
STAT3
TGFBR2
CASP8
SDHB
PPM1D
CYP17A1
MAP3K1
BAX
NTRK1
CDKN1A
ERCC3
VEGFA
CYP19A1
MDM2

ESR2	MAP2K1
HNF1A	EGF
EP300	IGF1
MAPK1	CASP3
NF2	PPP2R1A
RUNX1	MMP9
ATR	GSTP1
IL1B	NR5A1
JUN	SOD2
BCL2	IRF1
HIF1A	ZEB1
RAD54L	NRG1
TGFB1	ROCK1
FAS	EZH2
TSHR	AFP
RHOA	FGFR1
KDR	RAF1
IL6	TYMS
FASLG	NFKB1
GNAS	ABCG2
IL2	CD44
AURKA	CREBBP
DHFR	IL1RN
TNF	IGF1R
PPARG	EPHB2
IGF2	MITF
PGR	BCL2L1
SRC	PTPN11
MMP2	KLK3
PRKAR1A	CXCR4
NFE2L2	DNMT3A
ABCB1	NOTCH1
PIK3R1	CYP1A1
CDK2	YAP1
TP63	FGFR4
PTGS2	BUB1
EXT1	MMP1
ITGB1	CAST
MUC1	AKT2
IDH1	MECOM
RRAS2	FLT1
JAK2	PCNA
BIRC5	IGFBP3
PARP1	PTK2

IFNG	SP1
IGF2R	CDK6
PLAU	MMP7
MGMT	TGFBR1
CBL	ZEB2
PIK3CG	CAV1
LHCGR	TLR4
NKX2-1	MAPK8
IL10	PRLR
CDK1	GLI1
ABCC1	RAC1
SMAD3	CTLA4
VEGFC	ABL1
DNMT1	BMP4
INS	CSF1R
IDH2	NCOA3
VDR	FN1
NQO1	PDGFRB
MAPK3	MCL1
ERBB4	TYMP
TNFRSF10B	FOS
CASP9	GPC3
SERPINE1	MAX
LEP	MAPK14
MMP14	SLC2A1
MTHFR	OGG1
STAT1	CCNB1
CHEK1	RELA
TOP2A	HSPB1
EGLN1	CYP1B1
CCND2	GSK3B
VIM	PLK1
DPYD	POU5F1
DCC	NFKBIA
CASP10	SETD2
PDCD1	CYCS
CCNE1	TOP1
FOXO3	RPS6KB1
AXIN1	NOTCH2
XIAP	EPHA2
FLT4	RARB
RIPK1	PIK3CB
HGF	HSP90AA1
B2M	INSR

SMAD2	ABCA1
FASN	NRP1
CCL2	HDAC1
NOS3	ETS1
FOXO1	RARA
NPM1	SIRT1
TLR2	ALDH1A1
CTSD	BECN1
BMP2	GAPDH
CYP3A4	PTHLH
ICAM1	ENO2
AKT3	ANGPT2
IL4	ABCC2
BTK	TUBB3
TGFB2	COMT
ANXA5	GJA1
MYCN	EPHB4
DNMT3B	DAPK1
XPO1	GNRHR
PROM1	ANXA2
AHR	TEK
ODC1	HSPA5
PRKCA	ENG
PRKDC	TTK
CBS	ITGB3
JAK1	MAP2K2
CCND3	CREB1
CDH2	PLCG1
PIK3CD	KITLG
GATA3	CDH3
KRT8	POLG
ITGAV	PRKCD
HMGB1	ITGA6
SPARC	LDHA
PAK1	CTSB
HDAC9	PTGS1
IL7R	ALB
ARAF	PDGFB
KRT18	NOS2
MMP3	HSD17B4
PRKACA	CDC42
IRS1	GRB2
MAD1L1	LMNA
WNT5A	CASP7

PKM	ITGA2
CLU	ACACA
CA9	TFRC
MAP2K4	BDNF
FOLR1	HSPA8
VRK1	DPP4
EDN1	UGT1A1
SOX2	SGK1
ITGA5	MYB
FGF1	TGFB3
PTK2B	EDNRA
HMGA1	SHH
NOTCH3	ALDH2
GATA2	SQSTM1
SOS1	NTRK3
FANCL	LIG4
IDO1	CYP11A1
AMHR2	TFAP2A
GATA4	ADAM17
CDC25A	LEPR
IL6R	CASP2
PLA2G2A	JAK3
RXRA	MME
TUBB	HSPA1A
ST14	KDM6A
JUP	MIF
ADIPOQ	WNT4
TXN	CYP24A1
CYP2E1	FGF8
ITGB4	GSN
ERG	JAG1
STAT5A	F2R
LOX	NCAM1
TKT	FOXP3
CD36	ENO1
CDC25C	HDAC6
EIF4E	PTPN12
CD40	FOLH1
ACTA2	FST
TNFRSF1A	CACNA2D1
APAF1	MYD88
HSPD1	VCAN
TGM2	CDH5
SYP	RRM2

CASP1	TNFSF11
EIF2AK3	HK2
KEAP1	CALR
ATRX	EPAS1
PIK3R2	TMPRSS2
AXL	MTAP
GRN	FBN1
LEF1	SLC19A1
ESRRB	TYR
AURKB	CHUK
MC1R	SOD1
HDAC2	ANXA1
CTSL	GHR
MDM4	CYP2D6
CFTR	CXCR2
SERPINA1	STAT5B
L1CAM	EPHA3
IL2RA	DDR2
GATA6	NFKB2
NR3C1	MPO
KLF4	HLA-DRB1
CASR	BIRC2
PDPK1	GLS
PTPN1	APOE
PLG	HMOX1
NGF	CD59
HNF4A	IKBKB
POR	CD55
PRKD1	HDAC4
POMC	CD46
DCN	KDM1A
WEE1	CSK
WNT1	ATP7B
CTCF	YY1
SMO	MAPK10
PMM2	RHO
NTRK2	AGER
MMP13	PRKAA1
FEN1	ACTB
MST1R	CAT
IL4R	TNFRSF1B
CD8A	NGFR
NOTCH4	AGTR1
CD4	TNC

PEBP1	HMGCR
RUNX2	MAP3K5
HPGD	PTK6
REL	DDIT3
CD247	LDLR
ALOX5	GZMB
BMPR2	PRKCE
CD28	POLH
MTR	NR4A1
BMPR1B	CD40LG
ALDOA	FLNA
STK4	PAX2
HDAC3	SLC16A1
PTPRC	HSF1
CSNK2A1	NOD2
TGIF1	CYP2C9
COL2A1	CYLD
NAMPT	MYLK
PDK1	HSP90B1
XBP1	BMP7
STS	MMP12
ACVR1	AHCY
CCR5	TNFRSF11B
ACTN4	LRP6
ITGA3	IL6ST
FGF10	COL1A1
DKC1	GLI2
FLT3	NT5E
PIK3C3	RHEB
LAMC2	ASNS
LIG1	SMARCA2
PLAT	GLUL
TCF4	TNFAIP3
POLB	ANPEP
ADAM10	PPARGC1A
RRM1	KMT2A
EHMT2	PRDX1
ATP7A	WNT3
CYP27B1	MAP2K3
RPSA	RASA1
SH2B3	BCR
KRT14	SYK
FURIN	PIN1
HSP90AB1	GNAQ

F5
AIFM1
F2
SSTR2
EIF2AK2
GNA11
ROR2
SIRT3
PRMT1
CBFB
EPOR
VCAM1
LIMK1
MSN
MCM7
TRAF6
MCM2
STAT6
HPRT1
CLDN1
WNT3A
ADAM9
GPI
CP
TTR
CTBP1
PON1
HNRNPA1
EPHA1
DSP
MECP2
ACE
WNT10B
REN
LIFR
MAPK9
CSF3R
ITGB6
GPX4
PTGER2
RPA1
CUL3
TNFRSF11A
FTO

MAPK7
COL18A1
DES
TPO
GUSB
FLI1
MMP8
YWHAE
HSPA9
PRKCB
GLI3
PIM1
TNK2
IL1R1
DVL1
PAX3
SLC2A4
NOG
SPRY2
TRAF3
APOB
MAPT
VCL
GATA1
SLC29A1
DLL4
BRD4
TRPV6
ADRB2
PRF1
PRKAA2
PRKAB1
NEK2
G6PD
UMPS
UBE2I
GGT1
VWF
ISG15
RALA
DDX3X
PROS1
TLR3
UCHL1

SMARCAL1	EIF4G1
TAP1	MTHFD1
USP7	CACNA1G
CDK5	HK1
KAT5	LRP5
HYAL1	VCP
CASP6	CSNK1E
KAT2B	BIN1
PSEN2	THBD
SEMA3A	UBE3A
LCK	MMP19
HDAC5	LRP1
STIM1	PRKCZ
PRKCQ	GALK1
PTPN6	PPP2CA
MYH9	GNAI2
PGK1	CDH11
ATF4	SMAD6
MBL2	RPL5
CTSK	XDH
COL4A2	AKR1B1
RXRB	ATP2A2
ARG1	USP8
RPS19	PHGDH
TF	TTN
SREBF1	COL4A1
WNT7A	CSNK1D
THBS2	IHH
FYN	KL
PSAT1	DUSP6
MAPK12	TPM1
UNG	RORA
HSPG2	PLA2G4A
PTH1R	RBPJ
CSNK2B	MAOA
CD19	CYP2C8
IL2RB	GSR
TLR5	FGF23
PLK4	CD79A
ADA	NR1H4
LYN	THRB
RPL11	ZAP70
IKZF1	MAP3K7
FCGR3A	EDNRB

PAX6
CFH
TUBA1A
GFAP
EEF1A2
PBX1
ERN1
TYK2
FOXA2
FKBP5
CDK8
FZD4
GJB1
PRKCG
EEF2
COL1A2
ACHE
SLC2A3
ELANE
KIF11
DRD2
TYRO3
KNG1
P2RX7
GNB3
GFRA1
C3
PSMB8
ABCB4
INPPL1
NLRP3
MS4A1
SLC22A5
CRKL
GDNF
FES
PAK2
SMC1A
NEDD4
CD27
TLR7
F7
COL5A1
CNR1

FGA
RYR1
SERPINC1
PRKACB
HSD11B1
PITX2
MAP2K6
MYOD1
MAPKAPK2
KDM3B
FUCA1
IKBKG
MFN2
APOA1
COL3A1
LMNB1
FBP1
CSTB
NFATC1
ASS1
ITGAM
KDM5C
TPT1
PSMB9
SERPINH1
RPS6KA1
FCGR2A
TUBG1
GRM1
PCSK1
RAB27A
ABCB11
GSK3A
PSAP
PLCG2
TNFRSF13B
SCD
GBA1
AGT
DNM1L
ACVR2B
RPS6KA3
IFIH1
IFNAR1

OPRM1	YWHAQ
FXN	CYP27A1
CA2	ITK
KAT2A	BMP1
TBP	UBE2N
USP9X	ITGB2
AQP1	TLR8
ATP1A1	TH
APP	SPTAN1
PRNP	MDH2
RAC2	MYH11
LRRK2	TMPO
THRA	CRYAB
ITGA2B	ABCA3
TBK1	MAPKAPK3
SLC2A2	NR2F2
ACP5	PLD1
F13A1	TRPV1
PNP	TLR1
NR3C2	LBR
SLC6A3	NPC1
SMPD1	SLCO1B1
ARHGEF2	DBH
LAMB1	RYR2
PARK7	KCNQ1
STAT4	ATF6
RPS6KA5	PPP1CA
KRT1	KCNN4
CAD	IMPDH2
ENPP1	NEDD4L
TYRP1	CAMKK2
SGPL1	HTR1A
KCNH2	MAP2K7
MAPK13	HUWE1
VIPR1	SCARB1
AKR1C4	DNM2
NFATC2	PSEN1
ITGA4	GLUD1
NEU1	F10
SNCA	TARDBP
IFNAR2	FBLN5
CD38	AURKC
OGT	GRM5
MALT1	SLC6A4

TUBB2A
AQP5
CPT1A
BCHE
GHSR
CAPN2
ECE1
ASAH1
MERTK
PLA2G6
LIPE
IFNGR1
UCP2
FTH1
IRF7
ITGAL
CFI
SLC9A1
HTR2A
HCK
PC
SIRT2
KLK1
DHCR7
CARD11
PDHA1
PCCB
SH2D1A
NTF4
ITPR3
ITCH
CASK
PCCA
DCTN1
CYP11B2
LYZ
UBA1
PTGDR
GPHN
GFPT1
CAMK2G
ACVRL1
MARK3
LPL

CALCR
DYRK1A
PNKP
PRKG1
SCNN1A
SCN5A
IRAK1
ACTA1
SUMO1
SMC3
FAH
HADHA
GABBR1
CAPN1
ENTPD1
TAF1
GRIN2B
RIGI
ACAT1
OTX2
P4HB
SMAD9
OXTR
KCNMA1
FTL
CDC45
ACE2
PRKAR1B
RDX
SCNN1B
MAP4K4
SLC12A2
ARSA
YWHAG
ALPL
ADCY1
MSTN
STAT2
HSD17B10
MVK
DMPK
ACTG1
PCSK9
ENPEP

KCNJ5	ALDH7A1
TAB2	TUBA4A
YWHAB	MYL2
DIAPH1	TUBB4A
ADAMTS13	ADK
ACTN1	ACAN
TRPC6	EPHX2
PRKAG2	FGR
SORD	FGB
ITPR1	CYBB
F8	ADORA2B
CHRM2	SCN10A
FECH	ADORA2A
PDE4D	GAD1
CAMK2D	PTPN2
FKBP1A	PDE3A
SLC11A2	FAAH
HTRA2	PIK3C2A
TRPC3	LCAT
SLC5A1	ACADM
CPS1	SLC11A1
TNNT2	DDC
SLC40A1	F9
NOS1	PTPRF
SCN9A	OGDH
IRAK4	FCGR2B
MC4R	GLA
GLB1	PDP1
SLC6A2	ALDH1A2
CETP	GLP1R
SYNGAP1	MYH6
PINK1	GAA
TBXA2R	DGAT1
SERPING1	NCSTN
PTPN22	CHAT
CASP14	ADSL
A2M	MAN1B1
FGG	LRP2
PROC	GRIK2
NRXN1	PPP3CA
ITGA7	RAB7A
CDON	TACR3
ALDH5A1	NCF1
LPIN1	KCNK9

ATXN3	SLC4A1
SERPIND1	CACNA1C
PKLR	OTC
PAFAH1B1	SLC6A8
C1S	PIKFYVE
ST3GAL5	CTSF
SLC12A5	SLC1A1
PLIN1	ATP1A3
PPIB	SPTLC2
SIGMAR1	GGCX
PFKM	AMPD1
GALNS	CAPN3
PDXK	F11
PLA2G7	GCK
AQP2	IDE
PAH	SLC6A9
HEXB	P2RY12
CES1	DHODH
CACNA1H	F12
TOR1A	GCH1
GLDC	MYH7
HCFC1	SLC4A4
IMPDH1	CHRNA4
PRKG2	NPR2
NR1H3	VLDLR
GABRB2	SLC18A2
SLC1A2	LAT
ABCC6	MYBPC3
PAK3	PYGM
STX1A	SLC1A3
ADCY5	CA1
ADORA1	GABBR2
CPT2	ATP2A1
ATP1B1	SERPINI1
CTH	GRIA1
SLC25A4	NMNAT1
CYBA	NCF4
CFB	CHRNA2
PIP5K1C	TPH2
TNNI3	NPHS1
ADRA1A	CACNA1S
ADRB1	CACNA1A
VKORC1	KCNJ2
CTSA	PCK1

SLC6A1
DNM1
PCYT1A
GRIA3
GRIA2
GAMT
SNAP25
HTR7
DLG4
GABRB3
DCX

Supplementary Table S3: Common targets between juglone and ovarian cancer.

IDO1
CTSD
MAOA
CDC25C
CSNK2B
THRA
CDK5
STAT3
SLC2A1
HDAC2
TOP2A
EGLN1
XDH
TTR
CDK1
GUSB
MIF
TBXA2R
NR3C2
ABCC1
MME
SERPINE1
CDK2
NTRK3
TLR8